The Report Committee for Xiao Luo
Certifies that this is the approved version of the following report:

Experimental Studies on the Reservoir Dynamics of Water-based and Gas-based Fracturing Fluids in Tight Rocks

APPROVED BY
SUPERVISING COMMITTEE:

Supervisor: _____

David DiCarlo

Co-Supervisor: _____

Quoc Nguyen

Experimental Studies on the Reservoir Dynamics of Water-based and Gas-based Fracturing Fluids in Tight Rocks

by

Xiao Luo, B.S.

Report

Presented to the Faculty of the Graduate School of

The University of Texas at Austin

in Partial Fulfillment

of the Requirements

for the Degree of

Master of Science in Engineering

The University of Texas at Austin

May 2017

Dedication

To my parents, their love, support and encouragement had made this possible.

Acknowledgements

I would like to express my sincere gratitude to my supervisor, Dr. David DiCarlo for offering me the opportunity to work in the research group as well as his persistent support and guidance. I would like to thank Dr. Quoc Nguyen for the insightful comments and support. I would like to thank Shell-UT Unconventional Research and Foundation CMG for their financial support to this work.

My sincere thanks to my colleagues, Dr. Tianbo Liang and Dr. Rafael Longoria, who introduced the topic to me and helped me to overcome the challenges in my research. I would like to thank the staff members, Mr. Glen Baum and Mr. Gary Miscoe for their help. I want to thank Mr. Daryl Nygaard for his exquisite craftsmanship. My special thanks to Dr. Oualid M'Barki and Dr. Xiongyu Chen for their support and friendship.

Abstract

Experimental Studies on the Reservoir Dynamics of Water-based and Gas-based Fracturing Fluids in Tight Rocks

Xiao Luo, M.S.E.

The University of Texas at Austin, 2017

Supervisor: David DiCarlo

Co-Supervisor: Quoc Nguyen

Low permeability formations, including shale and tight reservoirs, have contributed over 50% of U.S. annual oil production. Many of these formations are oil productive formations, they include Bakken, Eagle Ford, Marcellus, Permian, and Utica. In order to obtain economic production, large amounts of fracturing fluids are consumed during the hydraulic fracturing treatments, but only a small fraction of the fluid is returned to the surface as flowback.

Water-based fracturing fluids may invade the rock matrix in a tight or unconventional reservoir and result in a water block that hinders oil production. To remedy this possibility, gas- and foam-based fluids have been developed. For an oil productive formation, the invasion of gas can also result in oil permeability reduction, i.e. a gas block, but the mechanism and clean up are likely to be different than a water block. As the two fluids exhibit different wetting nature, it is not clear how they compare to each other in a multi-phase flow perspective, such as their impact on the productivity in the short and long term.

In this work, we conduct experimental studies the reservoir dynamics of invaded fracturing fluids, reduction in the hydrocarbon permeability, and potential mitigation for cleaning up the fluid block. We scaled down this fluid invasion problem to a laboratory core sample. Water and N_2 are injected into a rock matrix to mimic the invasion of slickwater and gas-based fracturing fluids, respectively. We studied the evolution of the oil productivity and flowback versus time during the oil production. The respective performances for different fracturing fluids under different conditions will also be investigated in this study.

Table of Contents

List of Tables

List of Figures

Chapter 1. Introduction

Unconventional hydrocarbon resources, such as shales and tight formation, contribute a significant share of the total U.S. gas and oil production. To achieve economical production, large amounts of water are injected to stimulate these low/ultra-low permeability reservoirs. Typically, only a small portion of the water injected is recovered to the surface as flowback. Asadi et al. (2002)reported the fluids flowback for numerous stimulated wells in the Codell formation, the fluids recovered is only 7% - 15.6% of the amount of fluid injected. This lost water can be mainly trapped within the rock matrix or the induced un-propped fractures; it may also accumulate within the fracture due to the effect of gravity (Agrawal & Sharma, 2013). Generally, as the main fracture propagates, there is a driving force for the pressurized slickwater to enter the rock matrix. The loss of water to the oil productive matrix result in a water block near the contact of the fracture surface that hinders the production. In a water-wet medium, the permeability reduction of a water block is mainly due to the higher water saturation near the boundary due to capillary discontinuity (Bennion et al., 1996; Liang et al., 2015).

To mitigate the potential permeability damage from slickwater, other different types of fracturing fluids are proposed as viable fracturing fluids. They include: gas (N_2/CO_2) based fracturing fluids and energized/foam fracturing fluids. It is widely accepted that stimulation with energized/foam-based fracturing fluids results in a higher flowback and better clean-up of the fracturing fluids (Chambers, 1994; Friehauf & Sharma, 2009). However, the use of foam does not eliminate fluid invasion. According to Ribeiro and Sharma (2012), the usage of gas or foam can result in multi-phase leak-off to the formation. The majority of the work on fracturing fluids selection focuses on shale gas production (Bang, 2007; Bennion et al., 1996; Burke et al., 2011; Mahadevan et al., 2007). However, for an oil productive formation, the invasion of gas can result

in oil permeability reduction, i.e. a gas block, but the mechanism and reservoir dynamics are likely to be different than a water block. As the two different fluids exhibit a different wetting nature, it is not clear how they compare to each other in a multi-phase flow perspective, such as their impact on the productivity in the short and long term.

In this work, water and N_2 gas are used as two different types of fracturing fluids. A three-step coreflood sequence is developed to mimic invasion and flowback of the fluids in an initially oil-rich formation. During the flowback step, we monitor the history of oil productivity and compare the oil permeability reduction at an early and late time of production. we further explore the effect of different reservoir conditions, including different initial water saturation and the phase behavior of reservoir oil, to the dynamic of the fluid block and the evolution of oil productivity over time.

Chapter 2. Background and Literature Survey

Background on Unconventional Gas/Oil Production:

According to the Annual Energy Outlook 2017 provided by U.S. Energy Information Administration (EIA), the annual crude oil production from tight reservoirs, including shale and chalk formations, contributes to over 50% of the annual U.S. oil production (EIA, 2017). Many of the shale plays in U.S. are oil productive formations, they include Bakken, Eagle Ford, Marcellus, Permian, and Utica. Based on their production forecast shown in Figure 1, the unconventional oil production from the major shale plays will continue the grow steadily over the next several decades.

Shale or tight formation typically consist of rocks with an average pore size from 10 nm to 100 nm (Sigal, 2015). The extremely small pores result in low or ultralow permeability of the rock matrix, which imposes great resistance for oil to flow out from the formation. It is difficult to economically produce oil from these formations through conventional methods. Thus, these reservoirs are often regarded as unconventional reservoirs.

Technologies such as horizontal drilling and hydraulic fracturing enable economical oil production from these unconventional reservoirs. During hydraulic fracturing, a large amount of pressurized fracturing fluid is injected to the formation rock to generate a fracture network. This process potentially enhances the oil productivity by increasing the exposure of the flow area to the wellbore. It allows the production to bypass the near-well bore damage which occurs during drilling or well completion (Economides & Nolte, 2000).

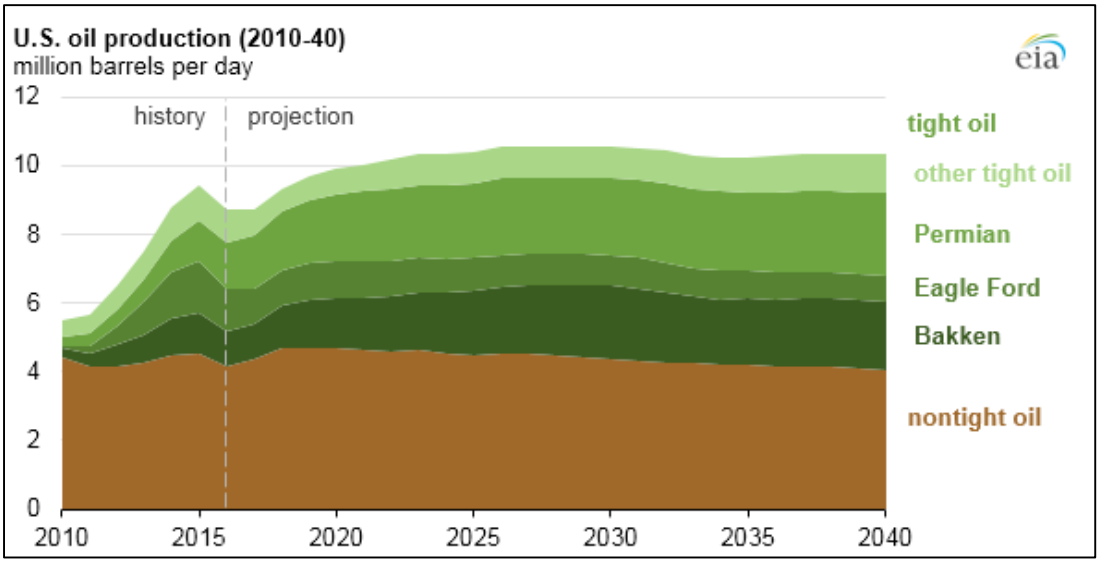

Figure 1. Total U.S. annual crude oil production and oil production from major shale plays (EIA, 2017).

Basic Properties of Shale Rock:

Shales are mudstones that are mainly composed of extremely fine sized particles with an average diameter less than 4 μm. The rock composition, such as clay, quartz, feldspar, etc., can vary significantly within the same shale play (Passey et al., 2010). As a porous media with ultralow permeability, its porosity and pore size distributions are potentially the two most important properties that impact the flow of hydrocarbon. As shown in Figure 2.A, a shale matrix consists of both organic and inorganic pores. The pore size is typically divided into three classes according to their size: 1) micropores with pore size below 2nm, 2) mesopores with pore size between 2 nm and 50 nm, 3) macropores with pore size larger than 50 nm. The fluid flow in each of the three classes is dominated by different mechanisms. For example, micropore filling, capillary condensation, and multilayer adsorption are more prominent in micropores, mesopores, and macropores, respectively (Kuila & Prasad, 2013). In addition to the complex pore system,

the wetting nature of the shale is important to understand the distribution of the fluid within the shale rock. Traditionally, the organic pores are considered to be oil/hydrocarbon-wet, where the inorganic pores are considered to be water-wet (Odusina et al., 2011). However, some recent studies have documented the existence of water in the organic pores which are considered to be hydrocarbon-wet (Chalmers & Bustin, 2010). Ruppert et al. (2013) studied the pore accessibility for water and methane through ultrasmall-angle neuron scattering technique. Their result showed that most of the pore are accessible to both water and methane, whereas pore smaller than 30 nm are more accessible to water. Although shale rocks are considered to be mix-wet, its affinity to water, particularly in the smaller pores, is likely to be underestimated.

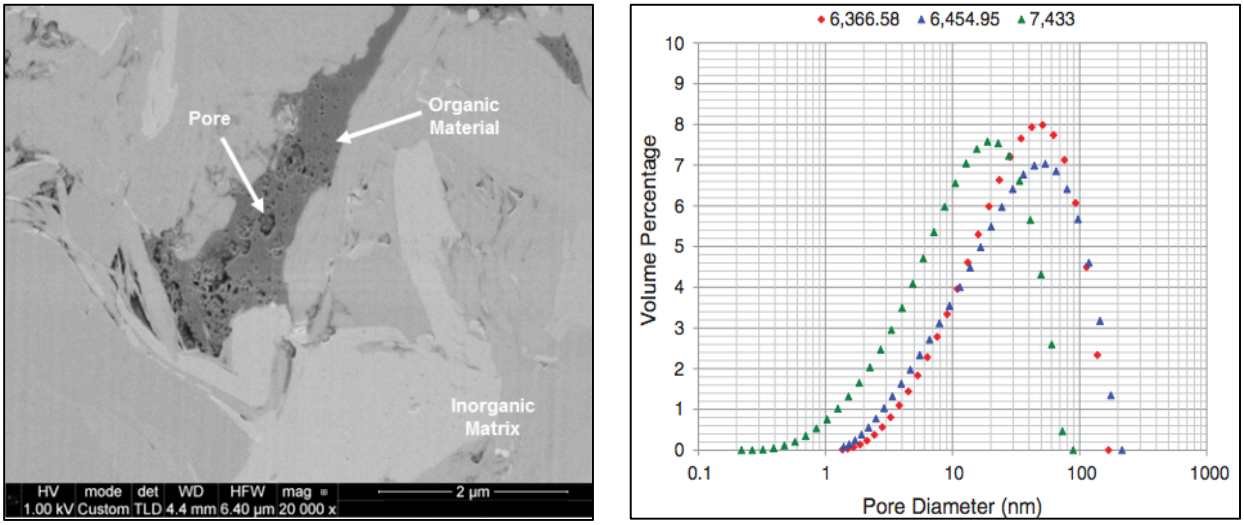

A B

Figure 2. A) SEM image of organic and inorganic matter for shales (Curtis et al., 2011). B) Pore size distribution for 3 different Bakken shale samples (Sigal, 2015).

Fracturing Network:

The stress state of the underground formation can be described by three unequal principle stresses, and fracture propagation is perpendicular to the direction with the least principle stress. This results in most fractures to be planar and their dimensions can be characterized by its

effective length, height, and width (Economides & Nolte, 2000; Fischer et al., 2008). The dimensions of the fractures are important aspect of the performance of a hydraulic fracturing treatment. The fracture length needs to propagate through sufficient reservoir volume to facilitate economic gas/oil production for shale or low permeability reservoirs. Mahrer (1999) reviewed numerous techniques to monitor fracture geometry. Some of the popular methods involve treatment-induced microseismicity observation from off-set wells and treatment pressure responses. Fisher and Warpinski (2012) has presented data for thousands of fracture treatments in major active shales play including Barnett, Woodford, and Marcellus. They concluded that the hydraulic fractures heights are relatively well contained and the in-situ stress contrasts between the shale layer and its overburden have the most significantly effect to the fracture height. The length and width of the fracture can depend on the optimization of the well productivity index after the treatment. The actually fracture half-length can be obtained through the history match of the well rate and pressure response during the stimulation treatment (Cipolla et al., 2008). The fracture half-length obtained through production analysis is usually shorter than the planned (Bybee, 2004). Lee and Holditch (1981) conducted pressure transient analysis on a hydraulic fractured, shale gas reservoir. Their results showed that the fracture half-length is 68% of the designed length, but the effective fracture half-length for gas production is only 5% to 11% of the designed length. One potential cause for the non-optimal performance of the fractured well is the presence of the fracturing fluid around the fractures. As demonstrated by Figure 3, This fluid reduces the relative permeability of hydrocarbon flow and significantly lower the effective fracture length (Lolon et al., 2003).

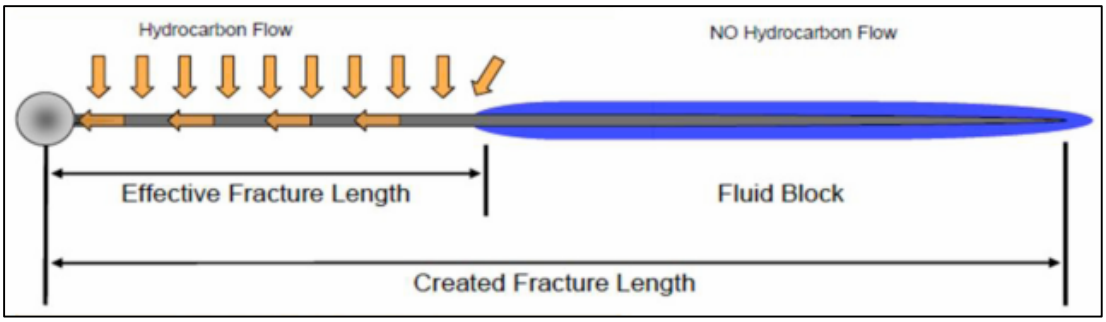

Figure 3. Effective fracture length and created fracture length. The fracturing fluids, colored in blue, blocked significant portion of the hydrocarbon flow, colored in yellow. (Soni, 2014).

Fluid Loss and Water Block:

Hydraulic fracturing of low permeability formations consumes large amounts of fracturing fluids, but only a small fraction of the fluid is returned to the surface as flowback. Asadi et al. (2002) provided a case study on the fracturing fluid flowback for numerous wells drilled in the Codell formation in the Denver-Julesburg basin. The reservoir is located at a depth of 7000 ft to 7200 ft. The permeability of the formation is below 0.1 mD and the porosity ranges from 8% to 20%. Various chemical tracer was used for each well to monitor the amount of the recovered fractured fluid. The sampling of the flowback lasts up to 18 hours depending hydrocarbon breakthrough. The amount of recovered fluids was obtained through the material balance for each chemical tracer. Table 1 shows the amount of recovered slickwater and the pumping schedule for the two wells with highest and lowest flowback efficiency, where the flowback efficiency is defined by the ratio of the amount of recovered fluids over the amount of injected fracturing fluids. For both wells, the amount of fluid injected was over 130,000 gallons per stage, and most of that was not recovered. Furthermore, the flowback efficiency at the early segment of pumping schedule is generally lower.

Both underachieved effective fracture length and low recovery of the flowback suggest that significant portion of the fracturing water are trapped after the treatment process. Based on some recent studies, the lost water is likely to invade rock matrix or accumulate within the fracture due to the effect of gravity (Agrawal & Sharma, 2013). Sharma and Manchanda (2015) showed that the water can also be trapped in the induced un-propped fractures. Regardless where the lost water is located, these trapped fluids can hinder the production of hydrocarbon and undermine the benefits of the fracturing treatment. During hydraulic fracturing, as the pressurized fracturing fluids facilitate fracture propagation, there is a driving force for the pressurized fracturing fluids to enter the rock matrix. This work will mainly concern the dynamic of the invaded fluids in the rock matrix.

Table 1: The flowback data for wells with the highest and lowest flowback efficiency (Asadi et al., 2002).

Segment	Injected fluid, gal	Flowback, gal	Flowback Efficiency, %
Gehring 8-15i6 (Total flowback efficiency, 15.6%)			
Pad	19000	1609.7	8.5
Pad	19000	1210.8	6.4
1 ppg	10000	1562.1	15.6
2 ppg	29000	3711.6	12.8
3 ppg	11000	1585.3	14.4
3 ppg	24000	4378.5	18.2
3 ppg	7500	1119.9	14.9
4 ppg	7500	2908.1	38.8
4 ppg	5000	2605.7	52.1
Flush	1428	85.7	6.0
Weber L4-6 (Total flowback efficiency, 4.7%)			
Pre-pad	19000	149.4	0.8
Pad	19000	34.4	0.2
1 ppg	10000	43.3	0.4
2 ppg	29000	93.4	0.3
2 ppg	11000	49.9	0.5
3 ppg	24000	1265.7	5.3
3 ppg	7500	694.8	9.3
3 ppg	7500	1566.8	20.9
4 ppg	5000	2324.4	46.5
Flush	1428	0.0	0.0

The invasion of water into the rock matrix results in water block. In the petroleum industry, hydraulic fracturing is not the only cause for the water block. Drilling and cementing also result in water block as water based fluids lost to the rock matrix (Clark & Barkat, 1990). The effect of water block to the gas production in shale and tight reservoir has been well studied and documented (Gruber, 1999; Holditch, 1979). Most gas productive formation exhibits strong capillary suction for water (Bennion & Thomas, 2005; Spencer, 1989). Most of the invaded water is trapped because the viscous force through drawdown is generally insufficient to overcome the capillary forces (Bennion et al., 2000). For a Corey-type gas relative permeability curve, the trapped water can significantly reduce the relative permeability of gas flow (Parekh & Sharma, 2004). Trapped water, as a wetting phase, potentially reduces hydrocarbon permeability in different ways. First, from relative permeability curves, any increase in water saturation would decrease the hydrocarbon permeability. Secondly, a higher water saturation is observed within the water invaded zone and near the fracture face, due to capillary discontinuity, resulting in a bottleneck for hydrocarbon production (Mahadevan & Sharma, 2003). This is shown in Figure 4. The capillary discontinuity arises from the continuity of the pressure of each flowing phase, and this discontinuity exists because the flow passes from the core with a finite capillary pressure within the core to the fracture with zero or negligible capillary pressure (Horie et al., 1990).

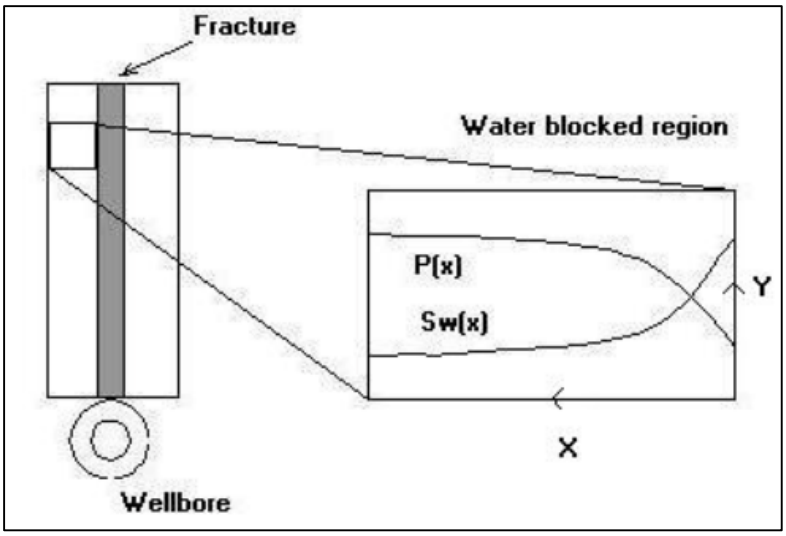

Figure 4. Water saturation and gas pressure profile in the invaded zone (Mahadevan & Sharma, 2003).

Richardson et al. (1952) demonstrated the boundary effect to the relative permeability curve for gas and oil flow at steady state. He was able to numerically compute the saturation profile by assuming a constant water saturation at the boundary. To investigate the boundary effect to coreflood experiments, Rapoport and Leas (1953) developed a dimensional scaling coefficient, $LV\mu\left[\frac{cm^2}{min}cp\right]$ also known as Rapoport & Leas number, based on generalized fraction flow theory at the core boundary. L is the length of the core in cm, V is the flux of the injecting phase in cm/min, and μ is the viscosity of the injecting phase in cp. Mathematically, the value of the coefficient determines the contribution of capillary pressure to the saturation profile near the boundary. They conducted multiple drainage experiments of waterflood on an oil-wet core with various scaling coefficients, and the recovery is strongly correlated to the scaling coefficient up to a critical value of 3 $\frac{cm^2}{min}cp$. In coreflood experiments, scaling coefficient greater than 3 is often applied to minimize the effect of capillary discontinuity. Experimentally, this can be achieved by increasing core length, injection rate or viscosity of the injected fluids. Holditch (1979)

concluded that water block can be cleaned up when the draw down pressure is much larger than the capillary pressure or the mobility of trapped water is high enough for water to imbibe into the formation. However, the drawdown pressure is often limited by reservoir pressure.

Other Fluid Loss and Fluid Block:

Although water-based fracturing fluids have been widely used for well stimulation. The treatment can result in a reduction of the hydrocarbon productivity. Different types fracturing fluids, i.e. energized or foam-based fracturing fluids, are developed to mitigate this possibility. This type of fracturing fluids consists at least one compressible component/phase. The term "energized fluids" generally refer to such fluids with quality below 52% and foam-based fracturing fluids generally exhibit a quality greater than 52% (Chambers, 1994). The use of energized or foam-based fracturing fluid can result in a multi-phase leak-off to the formation (Ribeiro & Sharma, 2012). For an oil productive reservoir, the invasion of the gas phase may also result in a gas block that hinders productivity reduction. However, the productivity reduction and clean-up of a gas block are expected to be different from a water block. Since the two fluids exhibit different wetting nature, it is not clear on how they compare to each other in the reservoir dynamics. In this work, we scale down the fluid block into a laboratory core sample. We implement a three-steps coreflood schemes to monitor oil productivity and the reservoir dynamics of lost fracturing fluids during flowback.

Chapter 3. Experimental Method

3.1 Experimental Approach

When fluids are injected at high pressure to fracture the rock, there is a driving force for fracturing fluids to enter the formation rock matrix. This will create a zone near the fracture face due to fluid invasion (Figure 5.A). This invaded zone may reduce the oil productivity during the production phase. The invasion of the fracturing fluids can be scale down to a laboratory core sample. Figure 5.B shows the similarities of fluid invasion at both field and laboratory scale. One of the core faces represents the contact surface, or the fracture face, between the hydraulic fracture and rock matrix. This approach enables us to explore the potential reservoir dynamics of the invaded fluid using through coreflood experiments. The permeability for hydrocarbon flow, which translates to hydrocarbon productivity, can be monitored through pressure drop measurements.

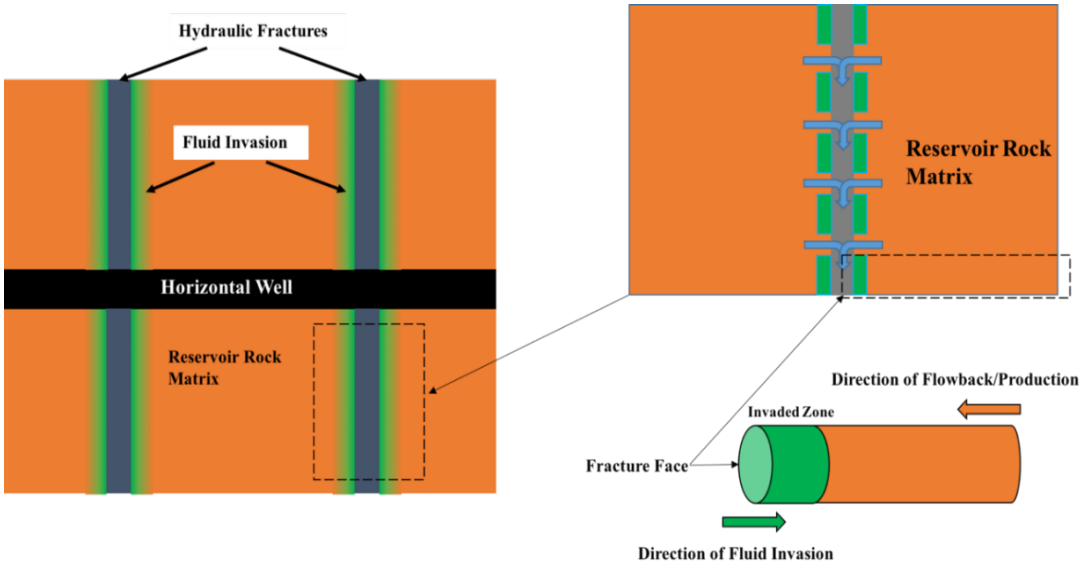

A B

Figure 5: Schematic of fluid invasion at different scale. A) Fluid invasion at field scale. B) Down scaling the invasion process to laboratory core process.

3.2 Materials

3.2.1 Core Samples:

We use Texas cream limestone (TCL) as a proxy for a tight carbonate rock. All our cores are drilled from the same block of Texas cream limestone outcrop. Our Texas cream limestone is a tight homogeneous water-wet rock. Its permeability is between 7 mD to 15 mD, and its porosity is around 0.265. We also use Indiana limestone (IL) in some of the experiments. The permeability for Indiana limestone ranges from 3 mD to 14 mD with a porosity at around 0.182. Although the two rocks may result in similar ranges of permeability and porosity, the water and oil relative permeability curves for the two rocks are expected to be different. All the cores are in a cylindrical shape with 1.5 inch in diameter and 9.5 inch or 11.4 inch in length. Although the permeability of our core is outside the value for a tight reservoir, it is low enough to result in

sufficient capillary force. This proxy core allows us to capture the relevant flow physics with the presence of significant capillary pressure. The core is cleaned and dried in a vacuum oven at 85 °C for no less than 8 hours before each use.

3.2.2 Invasion Fluids:

We use two different fluids as the invading fracturing fluids. To establish the water block during slickwater fracturing, we use DI water as the invasion fluid. To establish a gas block from immiscible gas or foam fracturing, we use nitrogen gas as the invading fluid.

3.2.3 Choice of Oil:

Low carbon number alkanes are selected to represent the hydrocarbon from productive shale and tight oil reservoir. To investigate the effect of gas and water block to oil production in low or ultra-low permeability reservoirs, we use n-heptane as a proxy light oil for all our core flood experiment. In addition, n-heptane does not alter the wettability of the limestone. N-heptane can dissolve nitrogen gas at our experimental condition. The equilibrium mole fraction (solubility) of nitrogen gas in the oleic phase is estimated to be 0.055 through a flash calculation using Peng-Robinson EOS with zero binary interaction parameters. In this work, we use regular n-heptane as gas-undersaturated oil and nitrogen-equilibrated n-heptane as gas-saturated oil.

The gas-saturated n-heptane is prepared by equilibrating the n-heptane with an excess amount of nitrogen gas in a piston accumulator. Figure 6.A shows the accumulator for oil equilibration with N_2 gas. As gas dissolves in the oleic phase, pressure inside accumulator decreases. The equilibrium pressure should be no less than the experimental pressure. Figure 6.B is the pressure history of the accumulation during the equilibration process. If pressure decays to 600 psi, the oil is re-pressurized to 800 psi to ensure gas dissolves to the oleic phase (see re-pressurization at a time of 24 hours). Once the oil is equilibrated, the accumulator is then positioned vertically. Water is injected from top to push the piston. The piston drives the excess gas and pushes oil through bottom exit.

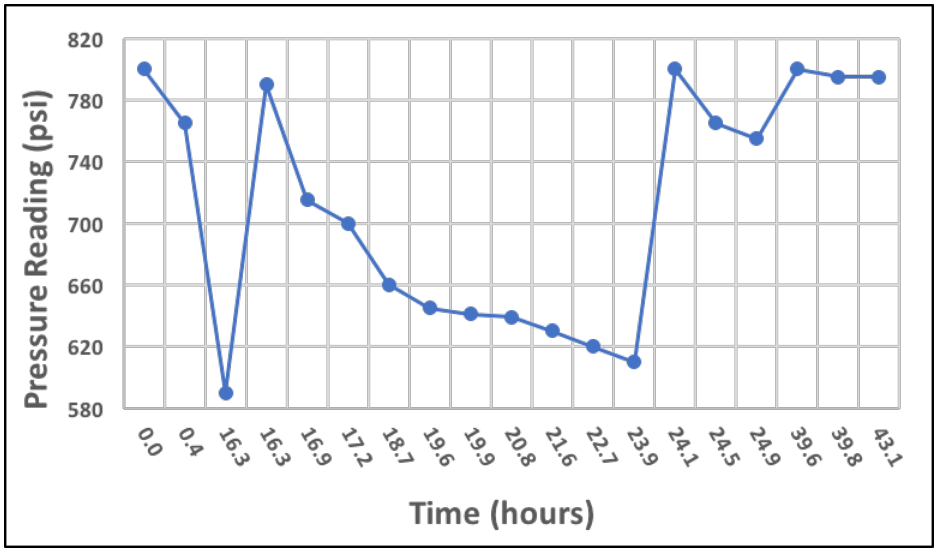

A B

Figure 6. A) Accumulator for oil equilibration. B) Pressure history inside the accumulator during oil equilibration.

3.3 Coreflood Schemes

3.3.1 Experimental Condition:

In Figure 7.A, a dry core is loaded into an aluminum Hassler-type core holder. The core along with the core holder is then connected with the experimental setup. All experiments are conducted at room temperature which is 24°C. A confining pressure of 1500 psi was applied around the core. The experimental pressure is maintained with a back-pressure regulator (BPR) at the downstream end. The schematic of the experimental setup is shown in Figure 7.B. Unless otherwise stated, the experimental pressure is at 600 psi. The core is vacuumed at -28 inHg gauge pressure for at least 2 hours to ensure most of the air within the core is purged before the experiment starts.

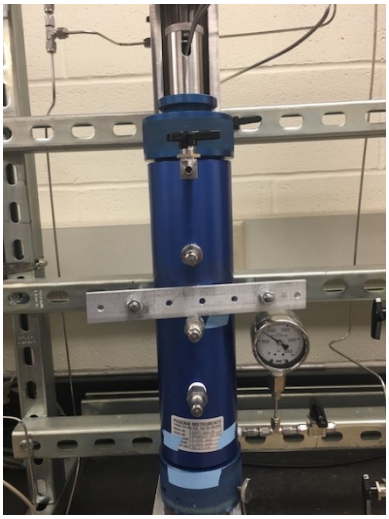

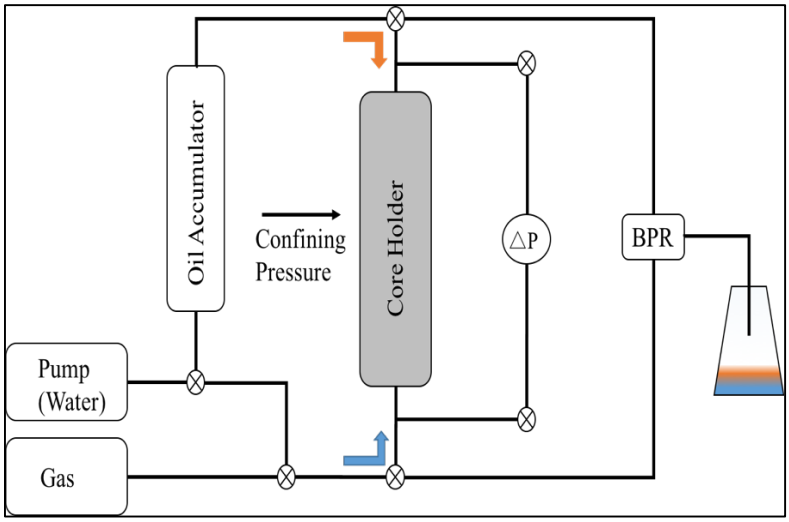

A B

Figure 7. Schematic of the experimental system. A) Hassler type core holder that is connected to the system. B) Overview of the experimental system. Blue arrow indicates the direction for water injection. Orange arrow shows the direction for oil injection.

3.3.2 Coreflood Sequence:

A coreflood experiment is designed to achieve the following steps: 1. establishing initial reservoir saturation, 2. fracturing fluid invasion, 3. flowback and oil production. During step 3, we measure the overall pressure drop across the core to monitor the oil permeability. As shown in Figure 8, a three step coreflood sequence is introduced below:

Step 1: Establishing Initial Reservoir Saturation

This step is to establish desired oil and water saturations within the core before the invasion step. Throughout this work, there are two different options of initial saturations: 1) a fully oil saturated core without any water. 2) a core that is saturated with both oil and water, but water phase is at residual water saturation. To achieve the former option, we simply inject oil directly to a vacuumed core. To achieve the latter option, the core is vacuumed then saturated with water. Then, a large amount of oil (greater than 10 pore volumes) is flooded through the

core. If no more water is observed at the effluent, then the initial condition is established. For either case, the overall pressure drop across the core is measured at various oil injection rates. This allows us to determine the effective permeability to oil base on Darcy's Law. If the core is fully saturated with oil, the overall pressure drop should reflect the absolute permeability of the core. If the core is at residual water saturation, the overall pressure drop corresponds to the end-point permeability for oil flow.

Step 2: Fracturing Fluid Invasion

A slug of fracturing fluid is injected to the core as the fluid invasion. Based on Figure 1B, the invasion fluid is injected from the fracture face of the core to mimic the fluid invasion in field scale. For gas invasion, the slug size is fixed at 10 mL which is 11% of the pore volume. This ensures that the invaded gas do not breakthrough the core while maintaining the same size of the invaded zone. For water invasion, different slug sizes were used.

Step 3: Flowback and oil production

Once the invaded zone is established within the core, oil is injected into the core to mimic oil production. The direction of the oil injection is opposite to the fluid invasion to mimic the oil flow from the further part of the reservoir to the fractures. Unless otherwise specified, the oil injection is at a constant rate of 0.05 mL/min. This flow rate generally results in a pressure drop less than 10 psi across the core sample. The capillary number, which relates the viscous forces and capillary forces, can be expressed by the following equation:

$$N_c = 2.6784 * 10^{-7} \left(\frac{K\Delta P}{\sigma L}\right) \quad (1)$$

Using laboratory units, K is core permeability in mD. σ is the interfacial tension in dynes/cm. ΔP is the pressure drop across the core in psi. L is the core length in inches. Based on our experimental condition, this flow rate results in a capillary number no greater than $8*10^{-8}$. The

critical capillary number for the Texas cream limestone cores is at around 10^{-4} (Bang, 2007). Our coreflood experiments are conducted significantly below the critical capillary number to ensure the essential dominance of capillary forces on micro-scale positioning of the invaded fluids. During this step, the overall pressure drop is measured across the core to monitor the productivity of the oil.

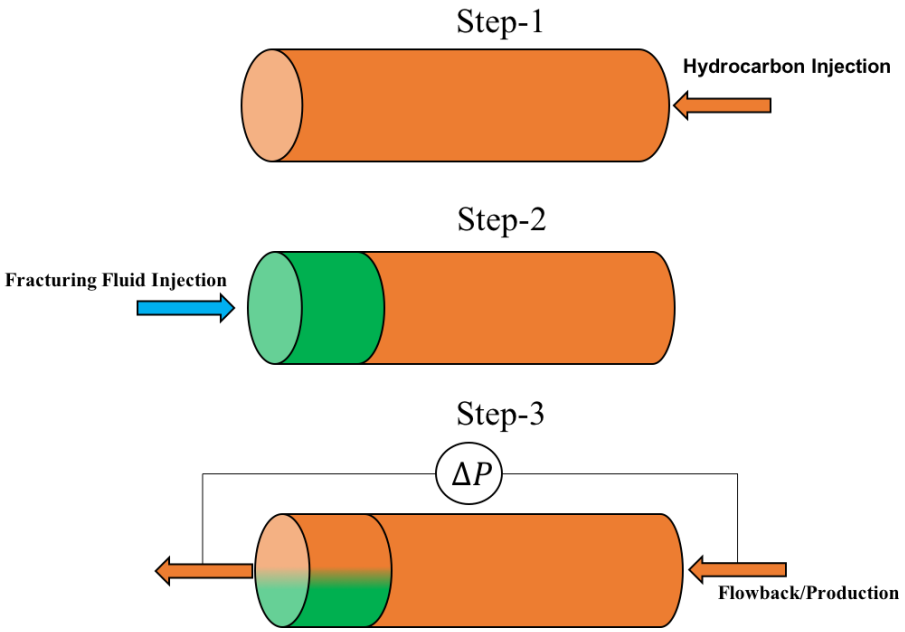

Figure 8. Cartoon demonstration of the 3-step coreflood sequence. Note that step-1 is subject to change depending on the desired initial saturation.

Chapter 4. Experimental Results

In this chapter, we choose water and N_2 as the invading fracturing fluids. Their dynamics within the core sample represent the reservoir dynamics of the lost slickwater and gas-based fracturing fluids respectively. We conducted fluid invasions to water-wet and fully oil saturated core. This means the initial water saturation is below its residual water saturation (Bennion & Thomas, 2005). This type of formation typically exhibits strong capillary suction due to significant capillary pressure at sub-residual water saturation. A fully oil saturated core is used to represent a desiccated reservoir. We conducted three different types of fluid invasions to our water wet rock. The three fluid invasions are water invasion, nitrogen gas invasion to gas-undersaturated oil, nitrogen gas invasion to gas-saturated oil.

Not all reservoirs are fully saturated with oil, their initial water saturation can be either at or above the residual water saturation. Since the initial reservoir condition can potentially influence the capillary forces and relative permeabilities. The reservoir dynamics of the invaded fracturing fluids needs to be evaluated. In this case, the core is initially at residual water saturation with respect to oil before the fracturing fluids invasion. We then follow similar steps with the first set of experiments and conducted the three types of fluid invasions.

4.1 Normalized Pressure Drop

To compare the oil permeability/productivity reduction from the fluids invasion, the measured pressure drop during flowback is normalized to the pressure drop prior invasion:

$$Normalized\ Pressure\ Drop = \frac{\Delta P_{after\ invasion}}{\Delta P_{prior\ invasion}} \quad (2)$$

where $\Delta P_{prior\ invasion}$ is the pressure drop of a certain oil flow rate before the fracturing fluids invasion, and is measured during step 1. $\Delta P_{after\ invasion}$ is the pressure drop of the same oil flow rate through the core with an invaded zone which is measured during step 3.

If the core is fully saturated with oil before the fracturing fluid invasion, then the pressure drop prior invasion corresponds to the absolute permeability. Similarly, if the core is at residual water saturation with respect to oil, then the pressure drop prior fluid invasion corresponds the endpoint oil permeability to water.

4.2 Results for Water Invasion

In this section, the same Texas cream limestone core is used. The pore volume of the core is measured to be 92 mL with a porosity of 0.26. The absolute permeability of the core is 10.2 mD. DI water is used as the invading fracturing fluid and n-heptane as the oil. Several water invasion experiments were conducted with Indiana limestone cores, with a pore volume of 41 mL and a porosity of 0.15. Their permeabilities range from 3 mD to 14 mD.

4.2.1 Water Invasion to Fully Oil Saturated Core:

The invaded zone is established with a 10 mL of water slug invasion to our Texas cream limestone core sample. The water invasion is immediately followed by the flowback and production step. Figure 9 shows the normalized pressure drop vs PV of oil injected during the production step. No water is observed from effluent for the duration of our pressure measurement. Thus, all of the invaded water remains in the core.

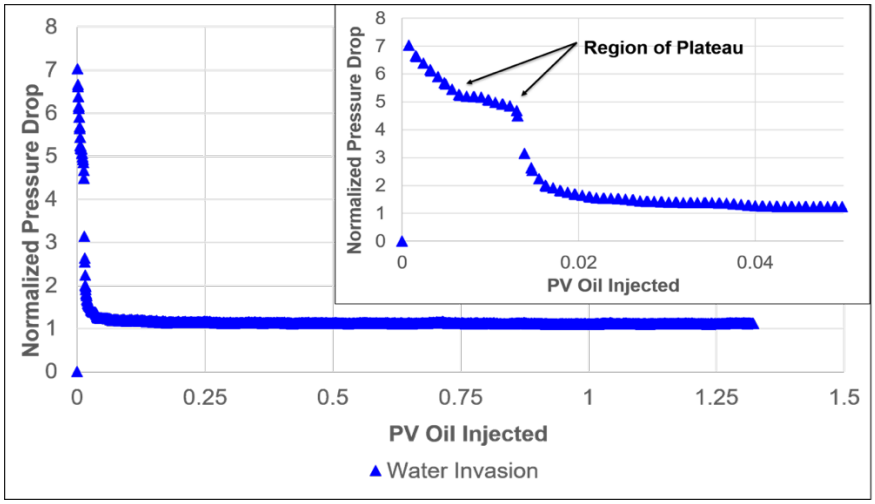

Figure 9. Normalized pressure drop for water invasion to fully oil saturated Texas cream limestone core.

In the zoomed plot, a pressure drop plateau is observed at the early time. The duration of the plateau is approximately 0.007 PV. The normalized pressure drop at the end of this plateau is 4.6. Liang et al. (2016) observed a similar plateau of much longer duration in their work. Near the end of this plateau, the normalized pressure drop rapidly decreases and settles at 1.1.

To demonstrate the evolution of the plateau duration, different slug sizes of water invasion are injected during step 2. The amount of the water invasion is chosen to be 10mL, 15 mL, 20 mL and 30 mL. The core is fully saturated with oil before invasion step. Figure 10 shows the normalized pressure drop during the flowback step. Table 2 summarizes some of the characteristics of each pressure drop history. The plateau duration grows significantly longer for with increases in the slug size of water.

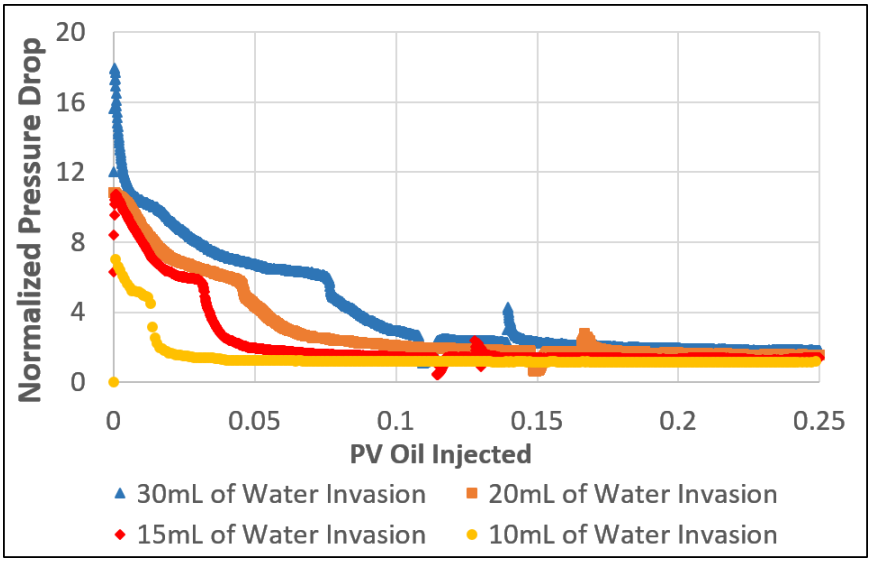

Figure 10. Different sizes of water invasion to a fully oil saturated Texas cream limestone core.

Table 2: Plateau durations and normalized pressure drop (NPD) for different sizes of water invasion to desiccated Texas cream limestone core.

Amount of Water Invaded	Estimated Plateau Duration (PV)	NPD at the End of Plateau	Late Time NPD
10 mL	0.007	4.6	1.1
15 mL	0.012	5.3	1.3
20 mL	0.022	5.6	1.4
30 mL	0.045	6.2	1.5

To show how both permeability and the invasion size can influence the plateau duration, the water invasion is experimented on different core samples. Here, we use Indiana limestone as our proxy core for water invasion. Figure 11 shows the evolution of plateau duration with different sizes of water invasion for an Indiana limestone core. Figure 12 shows the evolution of the plateau duration for Indiana limestones cores with different permeabilities. All the cores are

drilled from the same block but along different directions. The pore volumes and porosities are the same for all three cores. The plateau durations shown in Figure 11 and 12 are summarized in Table 3 and 4, respectively.

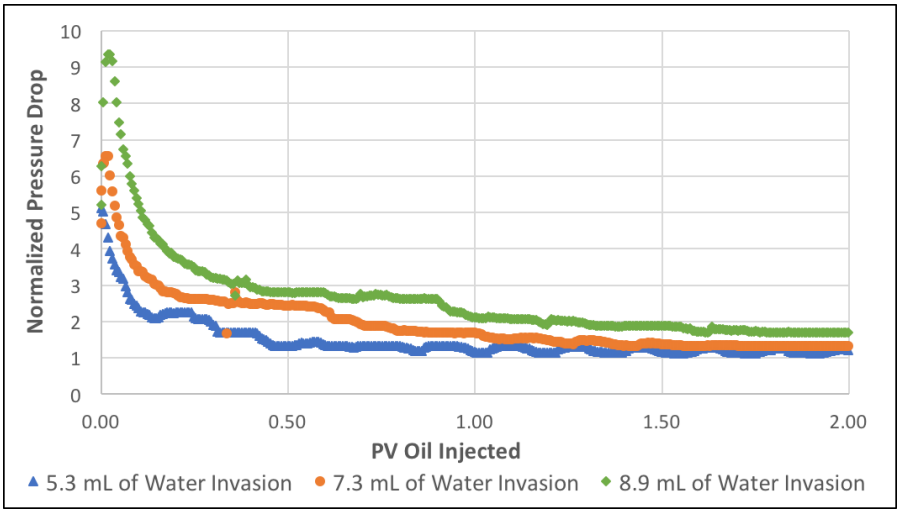

Figure 11. Different sizes of water invasion to a fully oil saturated Indiana limestone core. The core permeability is 7.1 mD.

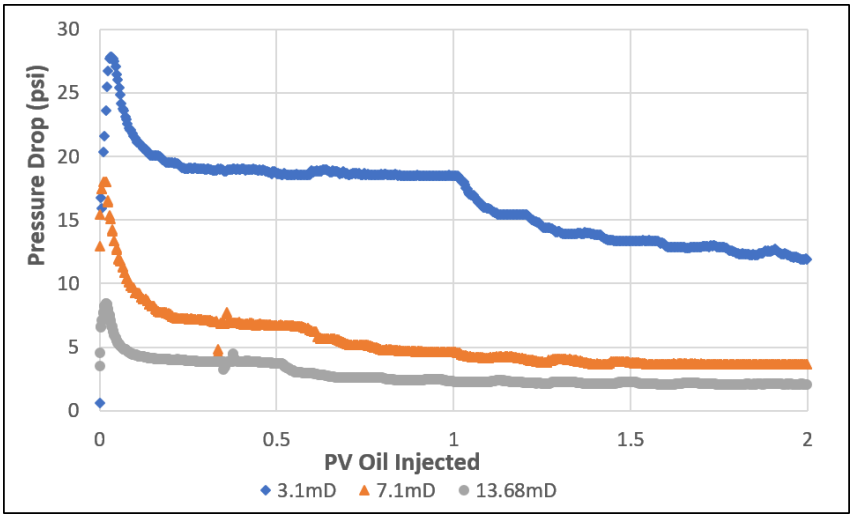

Figure 12. Same size of water invasion to fully oil saturated Indiana limestone cores with different permeabilities. The size of water invasion is 7.3 mL for all three cases.

Table 3: Plateau durations for different sizes of water invasion for Indiana limestone.

Amount of Water Invaded	Estimated Plateau Duration (PV)
5.3 mL	0.26
7.3 mL	0.59
8.9 mL	0.91

Table 4: Plateau durations for Indiana limestone with different permeabilities.

Absolute Permeability	Estimated Plateau Duration (PV)
3.1 mD	0.99
7.1 mD	0.59
13.7 mD	0.50

4.2.2 Water Invasion at Residual Water Saturation:

To show how a water block can behave differently at a different initial condition, the Texas cream limestone core is initially saturated with water. Oil is then injected through the core to displace the mobile water. The residual water saturation is reached when no more water is observed at the effluent for at least 1 PV of oil injected. The residual water saturation estimated to be 0.4 based on the water effluent collected downstream. Before water invasion, the initial saturation of the core is at its residual water saturation. 10 mL of water is injected as the invading fluid. The normalized pressure drop during the flowback is shown in Figure 13. Similar to previous water invasion, a plateau is present in the at the early time of oil production. The

duration of this plateau is approximately 0.08 PV. Near the end of this plateau, the normalized pressure decreased rapidly from 3.4 to 2.2, and then gradually decreases to 1.3.

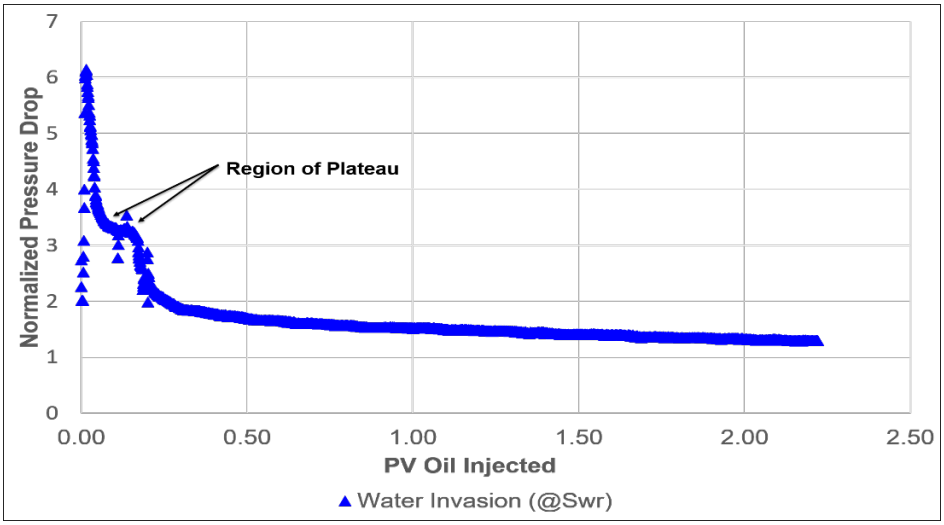

Figure 13. Water invasion to core with residual water saturation.

4.3 Results for Gas Invasion

The invasion of gas, as a non-wetting phase, is expected to impact the oil productivity differently than a water block. Here, we conduct experiments using gas as the invasion fluids and observe the pressure history during flowback. Same TCL is used with the water invasion experiments. We use N_2 gas as the invading gas-based fracturing fluid. Two different types of oil are used. The gas-undersaturated oil refers to the normal n-heptane. The gas-saturated oil refers to the n-heptane that is equilibrated with N_2 gas in section 3.2.3.

4.3.1 Gas Invasion to Gas-undersaturated Oil:

The core is initially saturated with regular oil (gas-undersaturated oil). 10 mL slug of nitrogen gas is injected into the core. As shown in Figure 14, the normalized pressure drop is initially at 1.5 and gradually decreases to 1 at approximately 0.5 PV of oil injection. This indicates that the oil permeability is fully recovered.

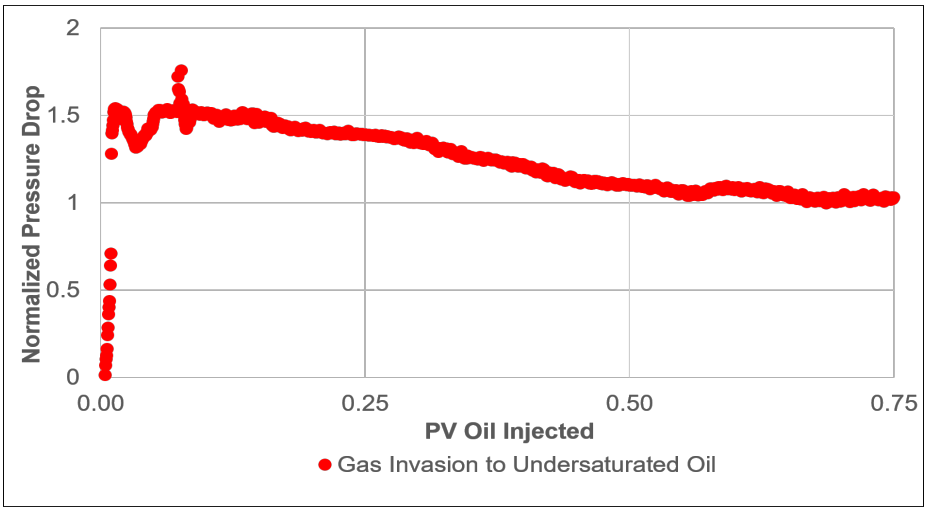

Figure 14. Normalized pressure drop for gas invasion to gas-undersaturated oil.

4.3.2 Gas Invasion to Gas-saturated Oil:

To demonstrate how gas solubility affects the clearing of the gas block, we use gas-saturated oil in this experiment. In the first step of the core flooding sequence, the core is saturated with regular (gas-undersaturated) oil. Then, gas-saturated oil is then injected into the core to displace the regular n-heptane. A minimum of 2 PV of gas-saturated oil is used to ensure the core is completely saturated with gas-saturated oil. The procedure for gas invasion is the same as described in the previous section. As shown in Figure 15, the normalized pressure drop begins at approximately 2 and decreases very slowly across the span of 1.5 PV of oil injection. The final value for the normalized pressure is approximately 1.8.

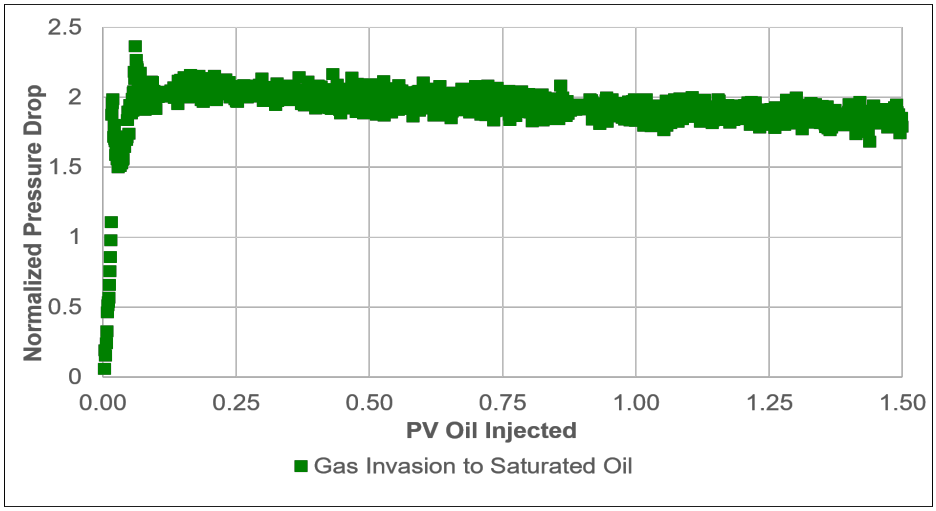

Figure 15. Normalized pressure drop for gas invasion to gas-saturated oil.

4.3.3 Gas Invasion to Gas-undersaturated Oil at Residual Water Saturation:

To see whether the residual water saturation assists or exacerbate the clearing of the gas block, the core is initially at residual water saturation with respect to regular n-heptane. A 10 mL slug of N_2 gas is injected into the core as the gas invasion. As shown in Figure 16, the normalized pressure drop decays from 2.7 to unity during the period of 0.5 PV oil injection. It reaches unity and stays constant, indicates the oil permeability reaches the end-point oil permeability to water. This is the maximum oil permeability that can be recovered with the presence of residual water. After this point, the normalized pressure drop stays constant at unity.

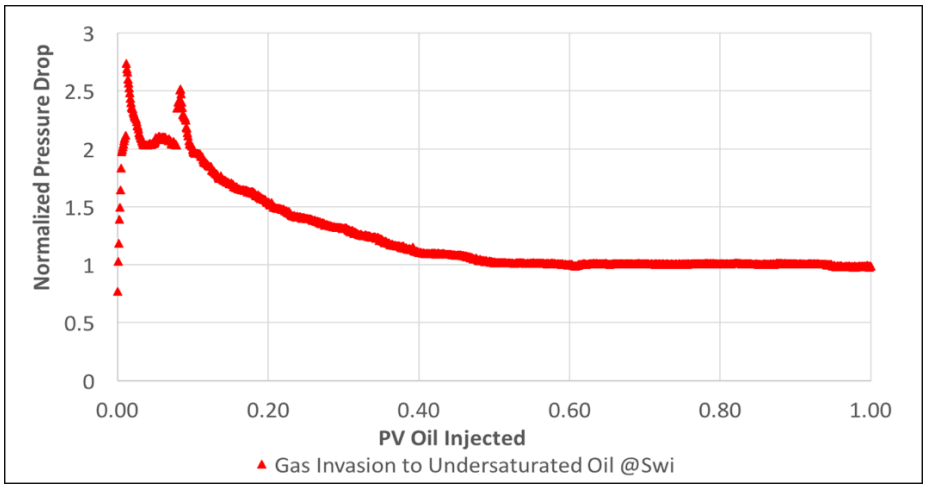

Figure 16. Normalized pressure drop for gas invasion to gas-undersaturated oil at residual water saturation.

4.3.4 Gas Invasion to Gas-saturated Oil at Residual Water Saturation:

Similar to the gas invasion in the previous experiment, the core is initially at residual water saturation with respect oil. 2 PV of gas-saturated oil is injected to the core to ensure the oil within the core is saturated with gas. Gas is then injected to the core as the invasion fluid. Figure 17 shows the normalized pressure drop during the flowback and production step. The normalized pressure drop increases rapidly to 3.5, then it stays almost constant. The steady state normalized pressure drop is approximately 3.3 which corresponding to the highest pressure drop among the experiments sets.

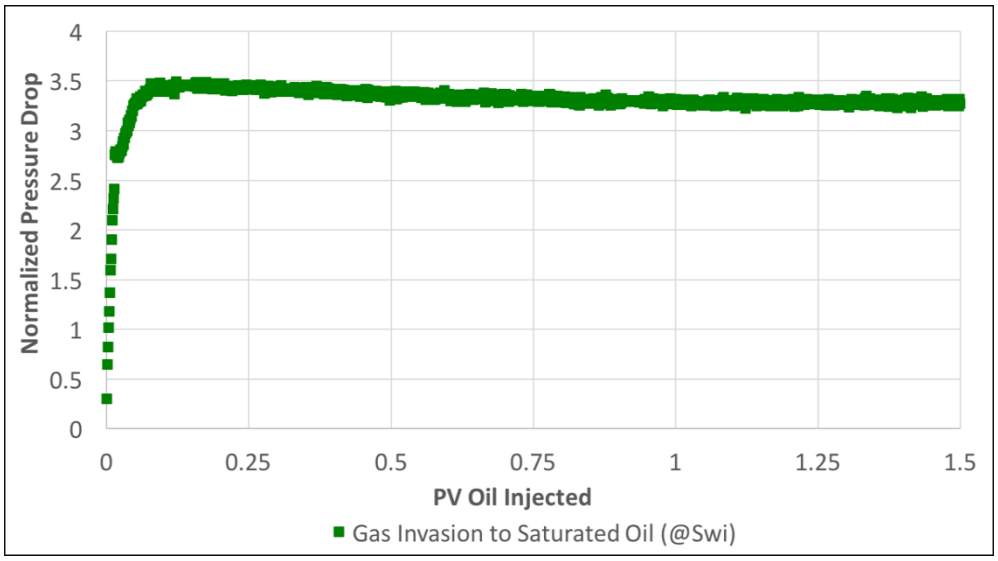

Figure 17. Normalized pressure drop for gas invasion to gas-saturated oil at residual water saturation.

Chapter 5. Discussion

5.1 Water Invasion Experiment

5.1.1 The Plateau Duration:

From the zoomed plot in Figure 9, the length of the plateau is 0.007 PV. The oil productivity reduction within the plateau duration is significant. The normalized pressure at the plateau is 4.6. This number corresponds to an oil permeability that is less than 25% of the original oil permeability. Since oil permeability rapidly recovers once plateau ends, this suggests that the plateau duration can be a characteristic time scale for clearing of the water block.

Based on Longoria et al. (2015) and Liang et al. (2016), the pressure drop plateau arises from the capillary discontinuity at the core face, where the water saturation there can be abnormally high. This results in a "bottleneck" hindrance effect to the oil flow. In addition, water may flow in opposite direction with oil due to counter-current imbibition. This process helps reduce the water saturation at the core face and leads to enhancement of the oil permeability.

Figure 18 is a cartoon of possible changes in the saturation profile due to imbibition of the water slug. The capillary force will redistribute the water saturation to an equilibrium state of uniform saturation throughout the core. The overall oil relative permeability is expected to change as the saturation profiles changes. The portion of the rock with highest water saturation generally dominates the overall oil permeability as its oil relative permeability is the lowest. In other words, the recovery of the oil permeability is physically related changes in the saturation profile saturation due to water imbibition.

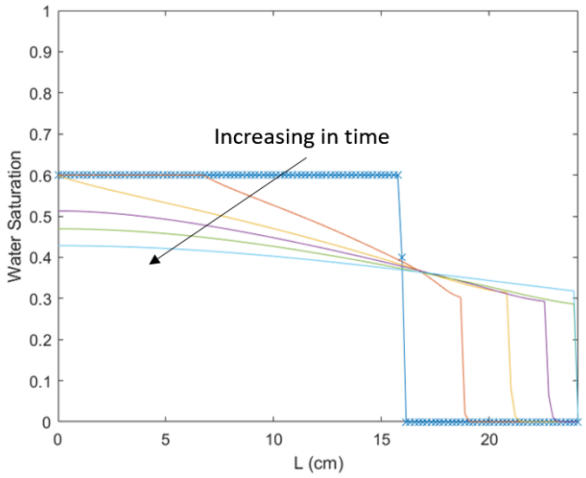

Figure 18. Illustration of the changes in the water saturation profile due to imbibition. The fracturing face is at L=0 cm.

This redistribution is modeled using the multi-phase flow equations and conservation of mass. Equation 3 is the governing equation for one-dimensional, unsteady, horizontal, two-phase flow for immiscible and incompressible fluids in a semi-infinite domain(Tavassoli et al., 2005):

$$\phi \frac{\partial S_w}{\partial t} + \frac{\partial}{\partial x}\left[\frac{\lambda_w \lambda_o}{\lambda_w + \lambda_o} K \frac{\partial P_c}{\partial S_w}\frac{\partial S_w}{\partial x}\right] = 0 \tag{3}$$

where λ_w and λ_o are the mobilities of water and oil, respectively. P_c is the capillary pressure between water and oil. K is the absolute permeability. ϕ is the porosity of the porous medium.

The Leverett J function can be applied to scale the capillary pressure.

$$J(S_w) = \frac{P_c(S_w)\sqrt{K/\phi}}{\sigma \cos\theta} \tag{4}$$

Combining Equations 4 and 3 yields:

$$\frac{\partial S_w}{\partial t} + \sigma \cos\theta \sqrt{\frac{K}{\phi}}\frac{\partial}{\partial x}\left[\frac{\lambda_w \lambda_o}{\lambda_w + \lambda_o}\frac{\partial J}{\partial S_w}\frac{\partial S_w}{\partial x}\right] = 0 \tag{5}$$

σ is the interfacial tension between the two fluids. θ is the contact angle. Let $\frac{\lambda_w \lambda_o}{\lambda_w + \lambda_o}\frac{\partial J}{\partial S_w} = D(S_w)$, then:

$$\frac{\partial S_w}{\partial t} + \sigma \cos\theta \sqrt{\frac{K}{\phi}}\frac{\partial}{\partial x}\left[D(S_w)\frac{\partial S_w}{\partial x}\right] = 0 \tag{6}$$

Equation 6 describe the counter-current imbibition process, its mathematical form resembles a non-linear diffusion type equation. Its solution can be written in the form of the following (Barenblatt et al., 2003; Birdsell et al., 2015).

$$u(t) = a/\sqrt{t} \tag{7}$$

where $u(t)$ is a characteristic flux of water imbibition. a is a constant. From Equation 7, it can be shown that:

$$t = bx^2 \tag{8}$$

where x is a characteristic distance and t is the time needed for water to move the characteristic distance. Comparing Equation 8 with 6, b contains the characteristic of the diffusion constant, and is proportional to $\sqrt{\frac{\phi}{K}}$. Let $b = \alpha\sqrt{\frac{\phi}{K}}$, then:

$$t = \alpha\sqrt{\frac{\phi}{K}}x^2 \tag{9}$$

α is a constant, which is dependent on core and fluids properties. If we let t represent the plateau duration, then x related to the depth of the water invasion.

$$x = \frac{V_{invaded}L}{1 - S_{or} - S_{wi}} \tag{10}$$

where $V_{invaded}$ is the amount of invaded water in PV. L is the core length. S_{or} is the residual oil saturation. S_{wi} is the initial water saturation which is 0 for a fully oil saturated core. For Indiana limestone cores, S_{or} is 0.4 and core length is 9.5 inches.

Equation 10 suggests that the plateau duration correlates linearly with $\sqrt{\frac{\phi}{K}}$ for constant invasion depth for the same rock type. It also suggests that the square root of plateau duration correlates linearly with different invasion depth for the same core. Figure 11 and 12 conveys the evolution of plateau duration with different invasion sizes and permeabilities, respectively. We extracted the plateau durations and plotted against different invasion depth and $\sqrt{\frac{\phi}{K}}$ values. This is shown in Figures 19 and 20.

Tables 5 and 6 lists the values of invasion depth, $\sqrt{\phi/K}$ and plateau duration. All values are converted in SI units so that α in Equation 9 can be evaluated independently from the fitted line with proper units. To evaluate α from Figure 19, the square of the slope equals to the value of $\alpha\sqrt{\frac{\phi}{K}}$, and α is calculated to be 0.649 s/m. From Figure 20, α is calculated to be 0.681 s/m. The difference between the two values is 2.4% of their average value. We also exam α on the Texas cream limestone core. Its value is obtained from Figure 21 and is equal to 0.043 s/m. We obtain the consistent α values for the Indiana limestone cores from two independent experiments, whereas the α value for Texas cream limestone is significantly different from Indiana limestone. We speculate the difference in the α values for two different rocks is due to their different pore size distributions. The physical meaning of α is lumped with the core properties and fluids properties. For Indiana limestone, the model can be used to correlate the plateau duration with core permeability and water invasion sizes. Nonetheless, with the same amount of water invasion, the smaller the α, the shorter the plateau.

Table 5: Converted values of invasion depths with corresponding plateau durations in SI units.

Invaded Water (mL)	Invasion Depth (m)	$\sqrt{\phi/K}$ (1/m)	Plateau Duration (sec)
5.3	0.0496	$4.73*10^7$	6214
7.3	0.0683		14592
8.9	0.0832		22404

Table 6: Converted values of $\sqrt{\phi/K}$ and corresponding plateau durations in SI units.

Core Permeability (mD)	Invasion Depth (m)	$\sqrt{\phi/K}$ (1/m)	Plateau Duration (sec)
3.1	0.0683	$7.07*10^7$	22710
7.1		$4.73*10^7$	14592

13.7		$3.38*10^7$	11016

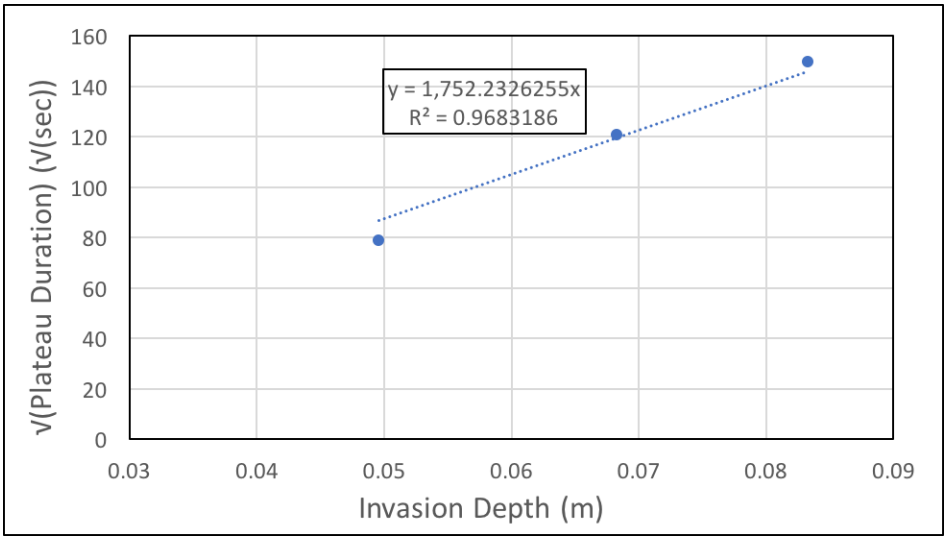

Figure 19. The square root of plateau duration versus invasion depth for Indiana limestone.

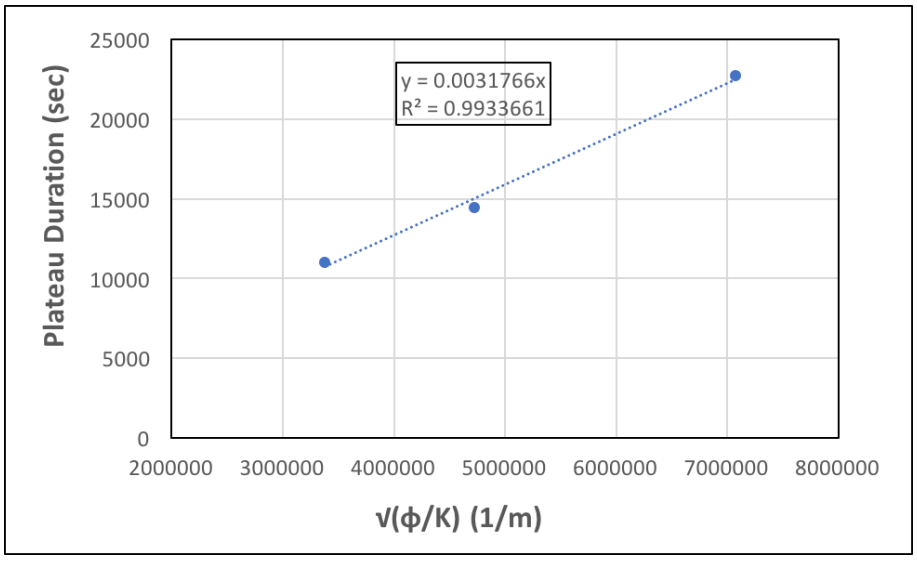

Figure 20. Plateau durations versus $\sqrt{\phi/K}$ for Indiana limestone.

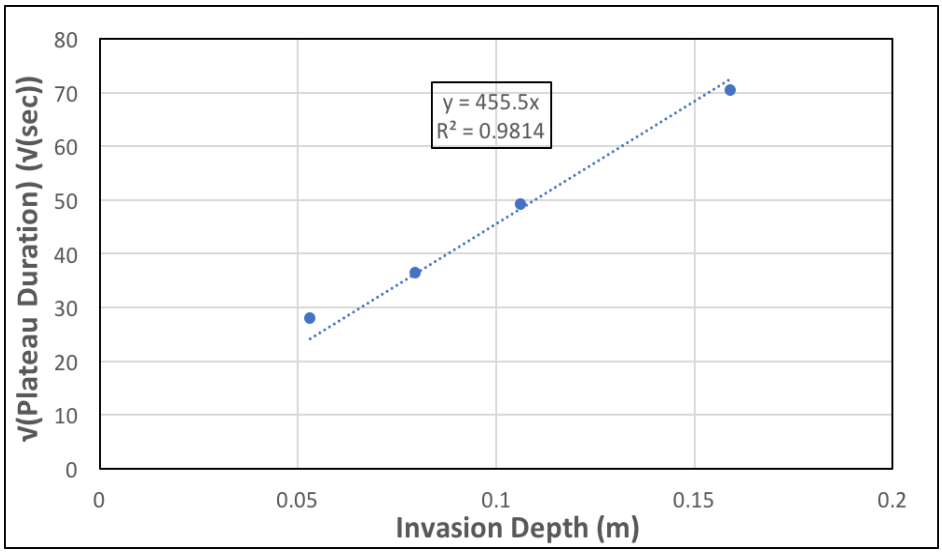

Figure 21. The square root of plateau duration versus invasion depth for Texas cream limestone.

We have shown how the plateau duration varies for different invasion sizes and core permeabilities using both experimental data and correlations. The short plateau duration in Figure 9 shows that capillary imbibition can be an effective mechanism to mitigate the water block. In Figure 10, this plateau duration increases to 0.08 PV with the presence of the residual water saturation. We speculate that the residual water increases the effective invasion depth and lower the capillary forces. Additional studies are required to determine which effect dominates.

5.1.2 Permeability Reduction at Long Term:

Imbibition of the water block allows the oil permeability to recover significantly. From on Darcy's Law, the reciprocal of the late time normalized pressure is simply the ratio of the oil permeability after the invasion to the oil permeability before the invasion. Figure 9 shows that the oil permeability can be recovered up to 90% of the absolute permeability when the core is initially fully saturated with oil. For the core that is initially at residual water saturation, the oil permeability is recovered up to approximately 80% of the end-point oil permeability. This is not surprising for a water-wet core since the endpoint permeability generally favors the non-wetting

phase. Despite the clearing of the water block at the late time, the oil permeability never recovers to the original permeability. This indicates a permanent permeability reduction due to the invasion of water.

5.2 Gas Invasion Experiment

5.2.1 Dissolution Time:

Both Figure 14 and 15 shows the results of gas invasion to a fully oil saturated core. The only difference between the two is that Figure 15 was obtained by using gas-saturated oil. We do not observe the pressure drop plateau which is shown in water invasion. The simplest reason for the difference is that the invaded gas, as a non-wetting phase, was unable to redistribute within the core. Therefore, capillary forces cannot mitigate the gas block for oil production.

Figure 14 conveys a transient permeability reduction when the normalized pressure drop decreases from 1.5 to unity at approximately 0.5 PV. This suggests that oil permeability fully recovers as the invaded gas was slowly dissolved away by the oleic phase. It is also important to point out that the normalized pressure drop decays almost linearly, suggesting a gas dissolution front is traveling along the core. The gas dissolution process can occur in both gas invasion and oil production step. Figure 22 is a simple schematic for the gas front during the gas invasion. To describe and model this front, we impose some basic assumptions, and they are listed below:

1. Constant temperature across the core.
2. Constant pressure across the core.
3. Gas invasion results in a piston-like shock front of the free gas phase with a constant gas saturation, S_g, behind the shock.
4. The amount of displaced gas is negligible compare to the dissolved gas. This implies that the gas is immobile and they leave the rock as dissolved gas.

5. Free gas phase is composed of pure nitrogen.
6. Local phase equilibrium can be applied.
7. No diffusion or dissolution across the gas front.

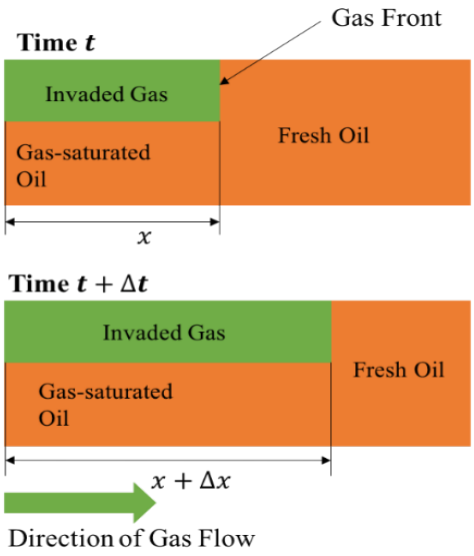

Figure 22: Schematic for the gas block during gas invasion step.

Using these assumptions, the calculations go as follows. Let n_{ij} denotes the moles of component i in phase j. For N_2 component, $i = 1$. For gas phase, $j = 1$. Similarly, n-heptane component and oleic phase correspond to $i = 1$ and $j = 1$, respectively. The overall mole balance on nitrogen component within the core is then:

$$(n_{11} + n_{12})_{t+\Delta t} - (n_{11} + n_{12})_t = \left[\left(\dot{n}_{gas}\right)_x - \left(\dot{n}_{gas}\right)_{x+\Delta x}\right]\Delta t \tag{11}$$

The oleic phase is fresh oil ahead of the shock; therefore, $\left(\dot{n}_{gas}\right)_{x+\Delta x}$, mole of N_2 component flowing out, is equal to 0. $\left(\dot{n}_{gas}\right)_x$ is molar rate of N_2 component entering the control volume. We can express the term n_{11} and n_{12} in terms of the volume of the corresponding phases. Because the gas phase can be regarded as pure nitrogen gas, then:

$$n_{11,t+\Delta t} = \frac{A\phi S_g(x+\Delta x)}{\underline{V_1}} \tag{12}$$

where A is the crosssectional area, ϕ is the porosity, $\underline{V_1}$ is the molar volume of the gas phase, which is N_2. S_g is the constant gas phase saturation behind the shock front.

n_{12} is the moles of dissolve gas in the oleic phase, and can be expressed as:

$$n_{12,t+\Delta t} = x_{12}\frac{A\phi\left(1-S_g\right)(x+\Delta x)}{\underline{V_2}} \tag{13}$$

x_{12} is the equilibrium mole fraction of N_2 component in the oleic phase and $\underline{V_2}$ is the molar volume of gas-saturated oleic phase.

The mole of gas entering the control volume is:

$$\left(\dot{n}_{gas}\right)_x \Delta t = \frac{q_{gas}}{\underline{V_1}}\Delta t \tag{14}$$

where q_{gas} is the in-situ volumetric rate for gas injection.

Similar expression can be derived for $(n_{11}+n_{12})_t$, and combine Equations 12-14 into Equation 11 and solve for $\Delta x/\Delta t$:

$$\frac{\Delta x}{\Delta t}_{invasion} = \frac{u_{gas}}{x_{12}\frac{\underline{V_1}}{\underline{V_2}}\left(1-S_g\right)+S_g} \tag{15}$$

where $u_{gas} = \frac{q_{gas}}{A\phi}$. Equation 15 can be used to estimate the velocity/position of the gas shock during the gas invasion step, and is subject to the constrains of the assumptions listed.

During the flowback step, we assume all the N_2 exits the core as dissolved gas. This assumption neglects the viscous displacement of the gas phase. The derivation for the flowback step is similar to the invasion step, except that the oil is injected from the opposite direction and the shock front is referred as fresh oil shock. Figure 23 shows the schematic of the fresh oil shock. We refer this as the fresh oil shock since the fluid is in single oleic phase behind the shock.

The existence of this shock front can also be proved from overall fraction flow curve for a gas and oil flow system (Orr, 2007).

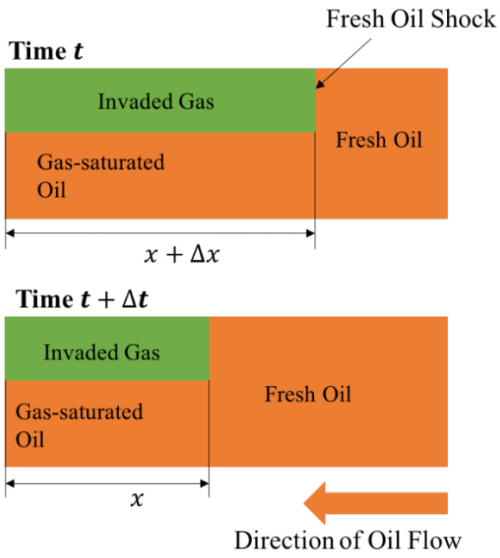

Figure 23: Schematic for the gas block during flowback step.

The material balance equation for the N_2 component is:

$$(n_{11} + n_{12})_{t+\Delta t} - (n_{11} + n_{12})_t = \left[\left(\dot{n}_{gas}\right)_{x+\Delta x} - \left(\dot{n}_{gas}\right)_x\right]\Delta t \tag{16}$$

The mole of gas present at time $t + \Delta t$ is the sum of the moles of the free gas and dissolved gas.

$$(n_{11} + n_{12})_{t+\Delta t} = \frac{A\phi S_g}{\underline{V_1}}x + x_{12}\frac{A\phi(1 - S_g)}{\underline{V_2}}x \tag{17}$$

The fresh oil shock is entering the control volume; therefore, there is no gas entering the control volume. $\left(\dot{n}_{gas}\right)_{x+\Delta x}$ is equal to 0.

$\left(\dot{n}_{gas}\right)_x$ is the rate of gas exits the core. Since there is no viscous displacement of gas by the oleic phase. Gas exits the core as the dissolved gas. Let $\dot{n}_2$ be the molar rate of oleic phase exits the control volume. We can express $\dot{n}_2$ as:

$$\dot{n}_2 = \dot{n}_{12} + \dot{n}_{22} \tag{18}$$

where $\dot{n}_{12} = x_{12}\dot{n}_2$. Combine this expression with Equation 18:

$$\left(\dot{n}_{gas}\right)_x = \dot{n}_{12} = \frac{x_{12}\dot{n}_{22}}{1 - x_{12}} \tag{19}$$

Note that $\dot{n}_{22}$ is the molar rate of oil component that exits the control volume. We express $\dot{n}_{22}$ in terms of the oil injection rate through the material balance on the oil component, then, substitute the expression for $\dot{n}_{22}$ into Equation 19. It eventually yields the following expression:

$$\left(\dot{n}_{gas}\right)_x = \frac{x_{12}q_{oil}}{(1 - x_{12})\underline{V}_{22}} + \left[x_{12}\frac{A\phi(1 - S_g)}{\underline{V}_2} - \frac{A\phi}{\underline{V}_{22}}\right]\left(\frac{\Delta x}{\Delta t}\right) \tag{20}$$

q_{oil} the in-situ volumetric rate for oil injection. $\underline{V}_{22}$ is the molar volume of pure n-heptane component. By substitute Equations 17-20 into Equation 16, the velocity of the fresh oil shock is:

$$\frac{\Delta x}{\Delta t}_{flowback} = -\frac{u_{oil}}{\frac{1 - x_{12}}{x_{12}}\frac{\underline{V}_{22}}{\underline{V}_1}S_g + 1} \tag{21}$$

where $u_{oil} = \frac{q_{oil}}{A\phi}$

To estimate the dissipation time of the gas block for our experiments, we first use Equation 15 to determine the position of the gas front by the end of the invasion step. Then, Equation 21 is applied to calculate how long does it take for the fresh oil shock to reach the fracture face of the core. The minus sign indicates that the shock is traveling in reserve direction to the invasion direction. Mathematically, by equating $\Delta x_{invasion}$ with $\Delta x_{flowback}$ can yield the following expression:

$$t_{recovery} = \frac{u_{gas}}{u_{oil}}\frac{\frac{1 - x_{12}}{x_{12}}\frac{\underline{V}_{22}}{\underline{V}_1}S_g + 1}{x_{12}\frac{\underline{V}_1}{\underline{V}_2}\left(1 - S_g\right) + S_g}t_{invasion} \tag{22}$$

where $t_{recovery}$ is the time for the fresh oil shock front reaches the exits of the core, it is also when gas block completely dissipation during the flowback step, and $t_{invasion}$ is the duration for gas invasion.

The model can be further extended to the case with initial immobile water with additional assumptions listed below:

1. A uniform immobile water saturation, S_{wr}, throughout the core.
2. Water is immiscible in the gaseous and oleic phase.
3. Presence of water does not affect the equilibrium of oleic and gaseous phase.

Following the same mathematical derivation, the final expression for shock velocity for the invasion step is:

$$\frac{\Delta x}{\Delta t}_{invasion} = \frac{u_{gas}}{x_{12}\frac{V_1}{V_2}\left(1 - S_g - S_{wr}\right) + S_g} \tag{23}$$

For the flowback step, the shock velocity is:

$$\frac{\Delta x}{\Delta t}_{flowback} = -\frac{u_{oil}}{\frac{1 - x_{12}}{x_{12}}\frac{V_{22}}{V_1}S_g + 1 - S_{wr}} \tag{24}$$

Compare Equation 24 to Equation 21, the presence of the residual water saturation increases the velocity for the fresh oil shock. Equation 23 and 24 can be combined to estimate the dissolution of the gas block based on the duration of the gas injection during the invasion step:

$$t_{recovery} = \frac{u_{gas}}{u_{oil}}\frac{\frac{1 - x_{12}}{x_{12}}\frac{V_{22}}{V_1}S_g + 1 - S_{wr}}{x_{12}\frac{V_1}{V_2}\left(1 - S_g - S_{wr}\right) + S_g}t_{invasion} \tag{25}$$

Equation 25 can be used to describe the dissolution of invaded gas into the reservoir oil. We can verify this time scale for the gas block to dissipate with our experiment results. From Figure 12 and 14, it takes approximately 0.5 PV of oil injection to clear the gas block. For both

experiment, duration of gas invasion is 40 minutes. Table 7 and 8 shows some measured values of the core properties and fluids properties. Using these values, the time required to clean up the gas block for fully oil saturated core is 907.2 minutes. For the case with initial water saturation, the time required is 945.8 minutes. The time for complete dissolution of the gas block are 0.50 PV and 0.52 PV respectively. These values are generally consistent with the experimental observations.

Table 7: List of core properties.

L	Core Length (cm)	28.96
A	Core Cross-sectional Area (cm^2)	11.4
ϕ	Porosity	0.275
S_g	Gas Saturation behind Gas Front	0.15
S_{wr}	Residual Water Saturation	0.40
K_{abs}	Absolution Permeability (mD)	11.5
K_{block}	Sectional Permeability Damaged by Gas Block (mD)	3.7

Table 8: List of fluid and flow properties.

$\underline{V_1}$	Molar Volume of Pure Gas (mL/mol)	595.74
$\underline{V_{22}}$	Molar Volume of Pure Oil (mL/mol)	147.37
$\underline{V_2}$	Molar Volume of Oleic Phase in Equilibrium (mL/mol)	132.01
x_{12}	Equilibrium Mole Fraction of Gas in Oleic Phase at Experiment Condition	0.055
q_{gas}	In-Situ Gas Injection Rate During Invasion (mL/min)	0.25
q_{oil}	In-Situ Oil Injection Rate During Flow-Back (mL/min)	0.05

The model allows us to obtain the length/size of the gas block once the position of the fresh oil is calculated. The overall oil permeability across the core can be estimated as the harmonic average of the damaged permeability and the absolute permeability, for a given the length of the damaged. In Table 7, K_{block} is the sectional permeability that is damaged by the gas block. Figure 24 conveys the pressure history obtained from the model and the experiment.

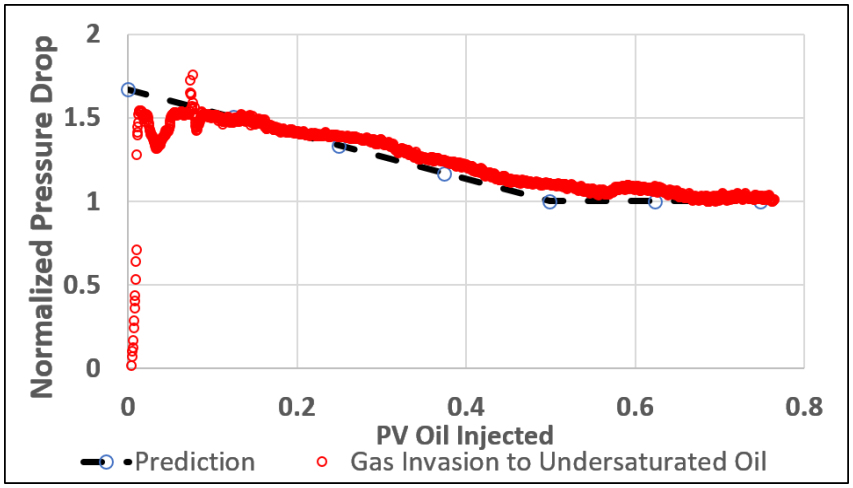

Figure 24. Pressure history obtained from model prediction and experiment for gas invasion to gas-undersaturated oil.

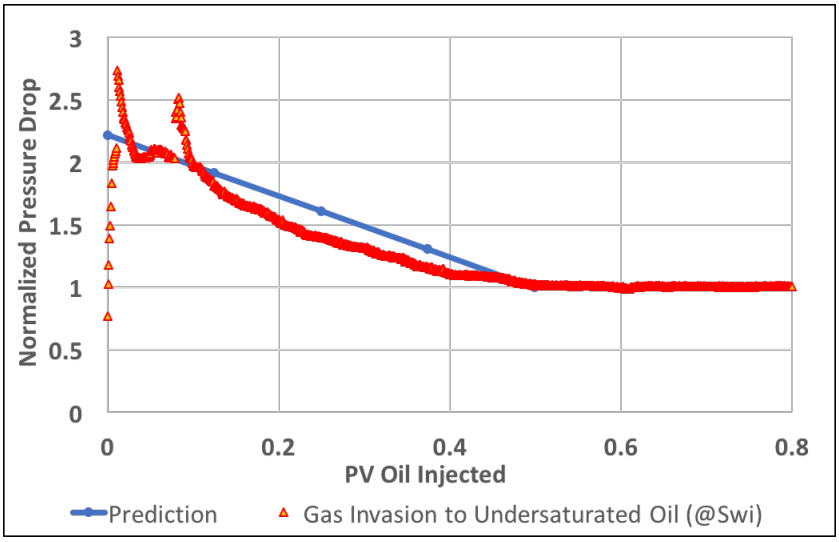

Figure 25. Pressure history obtained from model prediction and experiment for gas invasion to gas-undersaturated oil with residual water saturation.

In Figure 25, there are some deviations in the early pressure history between the model prediction and experimental data. We speculate there are some second-order effects, between the invaded gas and the residual water, influence the oil permeability. They are yet to be determined. Nonetheless, the model yields consistent predictions of overall dissolution time of the gas block.

When the gas-saturated oil is used, the gas block becomes permanent as no gas can dissolve in the oleic phase. The model shows a significant deviation in the normalized pressure drop. As shown in Figure 26, the experiment data conveys a less reduction of the oil permeability. We postulate two possibilities: the first possibility involves the reduction of the gas saturation. This can be achieved by gas displacement or latent gas dissolution (in case the oil is not fully saturated). The second possibility involves the self-mitigation that affects the gas saturation profile, such as capillary imbibition of the oleic phase. Despite the quantitative deviation in the permeability reduction, both curves suggest a permanent permeability reduction of the oleic phase at the long term.

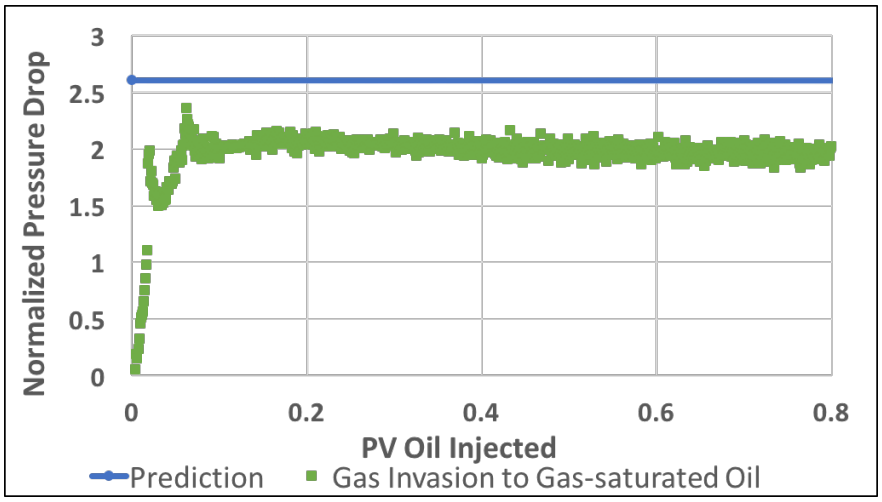

Figure 26. Pressure history obtained from model prediction and experiment for gas invasion to gas-saturated oil.

We further tested this model for low-pressure experiment condition. First, the solubility of the nitrogen is relatively low, the following approximation is valid:

$$\frac{1-x_{12}}{x_{12}} \approx \frac{1}{x_{12}} \tag{26}$$

Secondly, at low pressure, x_{12} can be obtained from Wilson's Correlation, which is based on Raoult's Law:

$$\frac{x_{11}}{x_{12}} = \frac{P_{c1}}{P} exp\left[5.37(1+\omega_1)\left(1-\frac{T_{c1}}{T}\right)\right] \tag{27}$$

where P_{c1}, T_{c1} and ω_1 are the critical pressure, critical temperature and acentric factor for the N_2 component, respectively. Since the gas phase consists of pure nitrogen, $x_{11} = 1$ and the temperature is taken as constant, this leads to x_{12} to be proportional to pressure.

$$x_{12} = \beta P \tag{28}$$

where β is the proportionality constant. The following expressing can be derived from the ideal gas law:

$$x_{12}\underline{V_1} = \beta RT \tag{29}$$

where $\underline{V_{11}}$ is the molar volume of pure nitrogen gas. R is the ideal gas constant. Equation 26 and 29 can be substituted into Equation 15 and 21. If the molar volume of the oleic phase is assumed to be constant with the change in pressure, then:

$$\frac{\Delta x}{\Delta t}_{invasion} = \frac{u_{gas}}{\frac{\beta RT}{\underline{V_2}}(1 - S_g) + S_g} \tag{30}$$

$$\frac{\Delta x}{\Delta t}_{flowback} = -\frac{u_{oil}}{\frac{\underline{V_{22}}}{\beta RT}S_g + 1} \tag{31}$$

Equation 30 and 31 convey the shock velocities are independent of system pressure. The overall dissolution times for the gas blocks are expected to be the same even at a different pressure. Figure 27 compares the gas block at 600 psi and 300 psi. The dynamics of the gas blocks are similar at different pressure conditions.

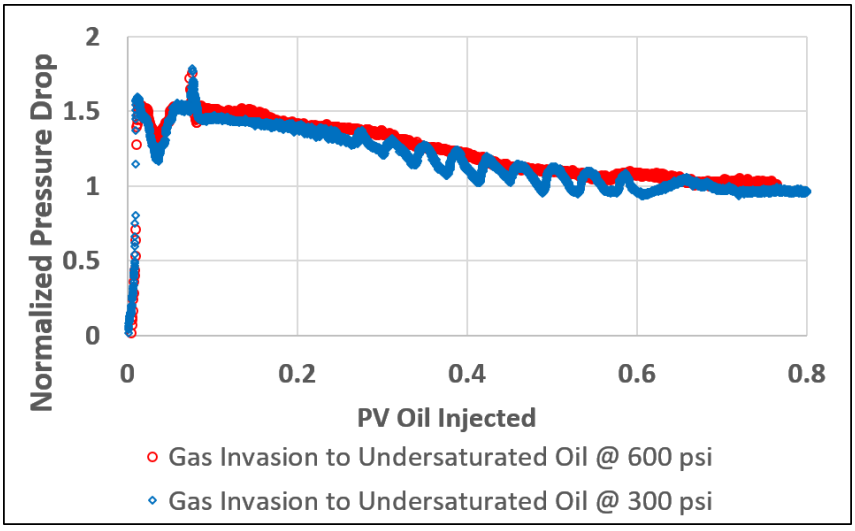

Figure 27. Gas invasion experiments conducted at different pressure conditions. The in-situ rates, q_{gas} and q_{oil} are the same for both experiments.

5.2.1 Permeability Reduction at Long Term:

Our model shows the transient oil permeability reduction is due to the dynamics of the gas block. A gas block can permanently reduce the oil permeability if it cannot dissolve into the reservoir oil. Both Figure 15 and 17 conveys a permanent permeability reduction by the gas block. The recovered oil permeabilities, in turns, are 56% and 30 % of the permeability prior invasion. As a non-wetting phase, the permeability reduction of gas is expected to be different than water. Our results suggest that the gas block reduces the end-point permeability for oil production in comparison with a water block of the same size.

5.3 Comparison of Gas and Water Invasion

Figure 28 compares of the fluid invasions to the fully saturated core. For gas-based fracturing fluids, the productivity quickly levels off depending on the gas solubility in the reservoir oil. For water-based fracturing fluid, the productivity increases rapidly but it does not recover to the undamaged productivity. Water- and gas-based fracturing fluids result in different types of permeability reduction during the production phase. This is because different physical mechanisms are responsible for the clearing of the fluid block: capillary forces for the water block and dissolution for the gas block. The water block clears up after the plateau duration, and the dissolution of the gas block is on a different time scale. For a fully oil saturated condition, capillary forces can be effective to facilitate the self-mitigation of the water block whereas the dissolution of gas does not attain a significant advantage with the absence of water. However, for long-term production, the oil permeability can be fully recovered from a gas block whereas a permanent permeability reduction from the water block. The solubility of the fracturing gas can

be an important factor affecting its performances. One subtle permeability reduction from gas block is that it lowers the endpoint permeability for oil flow.

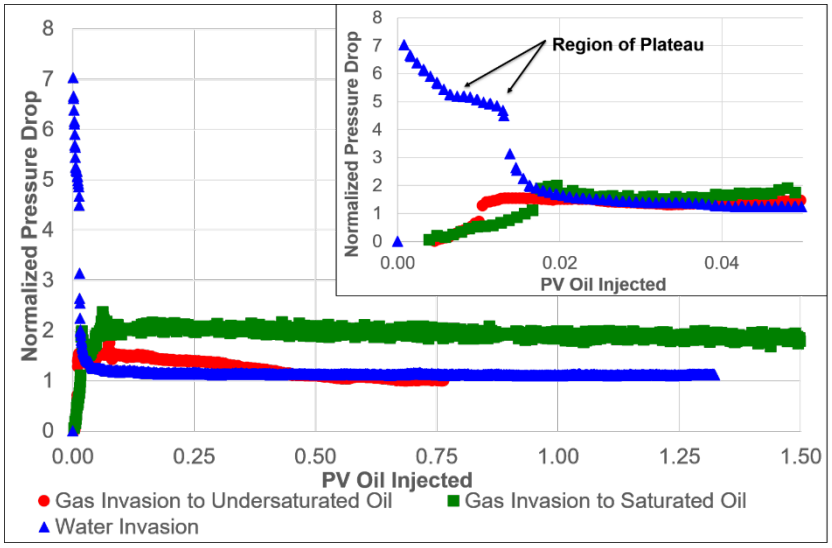

Figure 28. Comparison of water and gas invasion to fully oil saturated core.

The comparative performances of the fracturing fluids vary as their respective reservoir dynamics are influenced by the initial reservoir condition. As shown in Figure 29, when initially at residual water saturation, self-mitigation of the water block is significantly slower. On the other hand, the overall time scale for complete dissolution of the gas block is not impacted by the presence of water. This conveys that the gas-based fracturing fluid is favored in this case from the reservoir dynamics perspective. Again, the PVT behavior of the invaded gas and reservoir oil is critical to the evolution of oil productivity as governs the time scale when and whether or not the gas block can be cleared.

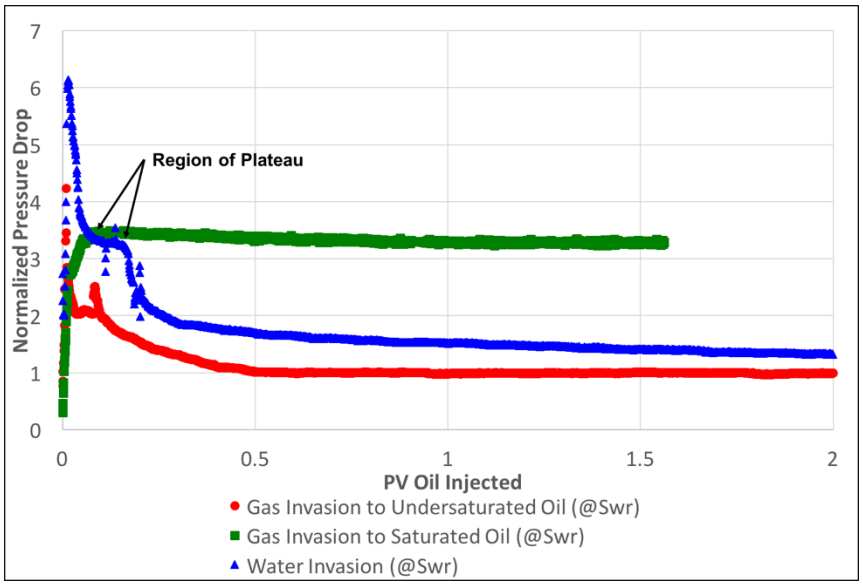

Figure 29. Comparison of water and gas invasion at residual water saturation.

Chapter 6. Conclusions and Future Work

6.1 Conclusions

This work concerns the effect of reservoir dynamics of lost fracturing fluids to the evolution of oil permeability in low permeability rocks. A coreflood scheme is introduced that allows us to mimic the fluid invasion and monitor the oil productivity history on laboratory core sample. Our results show that different fluids can cause different types of fluids blocks. Furthermore, different fluid properties and reservoir conditions result in different physical mechanisms for the self-mitigation for the recovery of oil productivity: capillary imbibition for water block and dissolution for the gas block. Correlations are developed to estimate the characteristic time scale on the clearing of either fluid block.

For a water-wet rock, the permeability reduction from a water block is mainly contributed by the high-water saturation near the fracture surface due to the capillary discontinuity. The effectiveness of self-mitigation for this water block is governed by the capillary forces. The time scale for the water block to clear depends on the capillary imbibition as well as the size of the water block. Any invaded water can cause a permanent increase in the water saturation and permeability reduction. But, as a wetting fluid, the oil permeability reduction from water block in long term is not as severe compare to a permanent block of a non-wetting phase.

The presence of the gas block can also reduce the oil permeability. Based on the PVT behavior between the fracturing gas and reservoir oil in question, gas-based fracturing fluids, if selected appropriately, can eliminate permeability blocks and facilitate complete permeability recovery. In the case when the gas block cannot be dissolved away, the trapped gas, as a non-wetting phase, can lower the endpoint permeability of oil.

In this work, we have shown that the reduction of the oil permeability from different fluids invasion is a dynamic process. The reservoir dynamics of the invaded fracturing fluids can impact the evolution of the oil productivity, and therefore, well economics. Thus, it should be considered during the selection between water- and gas-based fracturing fluids.

6.2 Future Work

In this work, we propose characteristic time scales for the self-mitigation of water block and gas block. They are the plateau duration for water block and the dissolution time for gas block. For water block, our model can be further improved by incorporating the effect of initial water saturation. For gas block, some of the assumption can be relaxed to include multi-phase flow, such as gas displacement.

As different fracturing fluids and formulations are developed to enhance the performance of a fracturing treatment, it would be interesting to extend this work to different types of fracturing fluids. One popular fracturing fluid is foam. As it consists of both liquid and gaseous phase, the multi-phase invasion can potentially result in both water and gas block. Their reservoirs dynamics, interfered by multi-phase flow, and the impact to oil productivity are yet to be studied.

The clearing of the fluid block is shown to be dependent on the amount of the fluid invaded. To accurately predicts the evolution of oil permeability, this work should be coupled with the research of fluid loss/leak-off.

The α values mentioned in Section 5.1.1 is shown to be different for different for each rock. One possible future work is to generalize this value for different rock type.

Unconventional reservoirs generally exhibit low/ultralow permeability that is below 100 nD, it is interesting to see how the experimental observations extrapolate to a lower range of permeabilities.

A more accurate quantitative comparison should include not only the time scales for the self-mitigation of the fluid block but also the permeability reduction before and after this time scale. Additional work is necessary to quantify the permeability reduction before plateau duration settles for water block and dissolution time for gas block.

Bibliography

Agrawal, S., & Sharma, M. M. (2013). *Liquid loading within hydraulic fractures and its impact on unconventional reservoir productivity*. Paper presented at the Unconventional Resources Technology Conference, Denver, Colorado, USA.

Asadi, M., Woodroof, R. W., Malone, W. S., & Shaw, D. R. (2002). *Monitoring Fracturing Fluid Flowback With Chemical Tracers: A Field Case Study*. Paper presented at the SPE Annual Technical Conference and Exihibition, San Antonio, Texas, USA.

Bang, V. (2007). *Development of a successful chemical treatment for gas wells with condensate or water blocking damage*: The University of Texas at Austin.

Barenblatt, G. I., Patzek, T. W., & Silin, D. B. (2003). The Mathematical Model of Nonequilibrium Effects in Water-Oil Displacement. *Society of Petroleum Engineers*. doi:10.2118/87329-PA

Bennion, D. B., & Thomas, F. B. (2005). Formation Damage Issues Impacting the Productivity of Low Permeability, Low Initial Water Saturation Gas Producing Formations. *Journal of Energy Resources Technology, 127*(3), 240-247. doi:10.1115/1.1937420

Bennion, D. B., Thomas, F. B., & Bietz, R. F. (1996). *Low Permeability Gas Reservoirs: Problems, Opportunities and Solutions for Drilling, Completion, Stimulation and Production*.

Bennion, D. B., Thomas, F. B., & Ma, T. (2000). *Formation Damage Processes Reducing Productivity of Low Permeability Gas Reservoirs*. Paper presented at the SPE Rocky Mountain Regional/Low-Permeability Reservoirs Symposium and Exhibition, Denver, Colorado, USA.

Birdsell, D. T., Rajaram, H., & Lackey, G. (2015). Imbibition of hydraulic fracturing fluids into partially saturated shale. *Water Resources Research, 51*(8), 6787-6796. doi:10.1002/2015WR017621

Burke, L. H., Nevison, G. W., & Peters, W. E. (2011). *Improved Unconventional Gas Recovery With Energized Fracturing Fluids: Montney Example*. Paper presented at the SPE Eastern Regional Meeting, Columbus, Ohio, USA.

Bybee, K. (2004). Hydraulic Fracturing: Fracture Half-Length From Design, Buildup, and Production Analyses. *Society of Petroleum Engineers*. doi:10.2118/0304-0041-JPT

Chalmers, G. R., & Bustin, M. R. (2010). *The Effects and Distribution of Moisture in Gas Shale Reservoir Systems*. Poster presented at the AAPG Annual Convention and Exhibition, New Orleans, Louisiana, USA.

Chambers, D. J. (1994). Foams for Well Stimulation *Foams: Fundamentals and Applications in the Petroleum Industry* (Vol. 242, pp. 355-404): American Chemical Society.

Cipolla, C. L., Lolon, E., & Mayerhofer, M. J. (2008). *Resolving Created, Propped and Effective Hydraulic Fracture Length*. Paper presented at the International Petroleum Technology Conference, Kuala Lumpur, Malaysia.

Clark, P. E., & Barkat, O. (1990). Analysis of Fluid-Loss Data. *Society of Petroleum Engineers*. doi:10.2118/18971-PA

Curtis, M. E., Ambrose, R. J., Sondergeld, C. H., & Rai, C. S. (2011). *Investigation of the Relationship Between Organic Porosity and Thermal Maturity in The Marcellus Shale*. Paper presented at the SPE North American Unconventional Gas Conference and Exhibition, The Woodlands, Texas, USA.

Economides, M., & Nolte, K. (2000). Reservoir Stimulation, 3rd, Schlumberger Ed: Services.

EIA. (2017). Annual Energy Outlook 2017. Retrieved from https://www.eia.gov/outlooks/aeo/tables_ref.cfm

Fischer, T., Hainzl, S., Eisner, L., Shapiro, S. A., & Le Calvez, J. (2008). Microseismic signatures of hydraulic fracture growth in sediment formations: Observations and modeling. *Journal of Geophysical Research: Solid Earth, 113*(B2), n/a-n/a. doi:10.1029/2007JB005070

Fisher, M. K., & Warpinski, N. R. (2012). Hydraulic-Fracture-Height Growth: Real Data. *Society of Petroleum Engineers*. doi:10.2118/145949-PA

Friehauf, K. E., & Sharma, M. M. (2009). *Fluid Selection for Energized Hydraulic Fractures*. Paper presented at the SPE Annual Technical Conference and Exhibition, New Orleans, Louisiana, USA.

Gruber, N. G. (1999). Water Block Effects In Low Permeability Gas Reservoirs. *Journal of Canadian Petroleum Technology*. doi:10.2118/96-92

Holditch, S. A. (1979). Factors Affecting Water Blocking and Gas Flow From Hydraulically Fractured Gas Wells. *Journal of Petroleum Technology*. doi:10.2118/7561-PA

Horie, T., Firoozabadi, A., & Ishimoto, K. (1990). Laboratory Studies of Capillary Interaction in Fracture/Matrix Systems. *Society of Petroleum Engineers*. doi:10.2118/18282-PA

Kuila, U., & Prasad, M. (2013). Specific surface area and pore-size distribution in clays and shales. *Geophysical Prospecting, 61*(2), 341-362. doi:10.1111/1365-2478.12028

Lee, W. J., & Holditch, S. A. (1981). Fracture Evaluation With Pressure Transient Testing in Low-Permeability Gas Reservoirs. *Society of Petroleum Engineers*. doi:10.2118/9975-PA

Liang, T., Achour, S. H., Longoria, R. A., DiCarlo, D. A., & Nguyen, Q. P. (2016). *Identifying and Evaluating Surfactant Additives to Reduce Water Blocks after Hydraulic Fracturing for Low Permeability Reservoirs*. Paper presented at the SPE Improved Oil Recovery Conference, Tulsa, Oklahoma, USA.

Liang, T., Longoria, R. A., Lu, J., Nguyen, Q. P., & DiCarlo, D. A. (2015). *Enhancing Hydrocarbon Permeability After Hydraulic Fracturing: Laboratory Evaluations of Shut-ins and Surfactant Additives*. Paper presented at the SPE Annual Technical Conference and Exhibition, Houston, Texas, USA.

Lolon, E. P., McVay, D. A., & Schubarth, S. K. (2003). *Effect of Fracture Conductivity on Effective Fracture Length*. Paper presented at the SPE Annual Technical Conference and Exhibition, Denver, Colorado, USA.

Longoria, R. A., Liang, T., Nguyen, Q. P., & DiCarlo, D. A. (2015). *When Less Flowback Is More: A Mechanism of Permeability Damage and its Implications on the Application of EOR Techniques*. Paper presented at the Unconventional Resources Technology Conference, San Antonio, Texas, USA.

Mahadevan, J., & Sharma, M. M. (2003). *Clean-up of Water Blocks in Low Permeability Formations*. Paper presented at the SPE Annual Technical Conference and Exhibition, Denver, Colorado, USA.

Mahadevan, J., Sharma, M. M., & Yortsos, Y. C. (2007). Evaporative Cleanup of Water Blocks in Gas Wells. doi:10.2118/94215-PA

Mahrer, K. D. (1999). A review and perspective on far-field hydraulic fracture geometry studies. *Journal of Petroleum Science and Engineering, 24*(1), 13-28. doi:http://dx.doi.org/10.1016/S0920-4105(99)00020-0

Odusina, E. O., Sondergeld, C. H., & Rai, C. S. (2011). *NMR Study of Shale Wettability*.

Orr, F. M. (2007). *Theory of gas injection processes*: Tie-Line Publications.

Parekh, B., & Sharma, M. M. (2004). *Cleanup of Water Blocks in Depleted Low-Permeability Reservoirs*. Paper presented at the SPE Annual Technical Conference and Exhibition, Houston, Texas, USA.

Passey, Q. R., Bohacs, K., Esch, W. L., Klimentidis, R., & Sinha, S. (2010). *From Oil-Prone Source Rock to Gas-Producing Shale Reservoir - Geologic and Petrophysical Characterization of Unconventional Shale Gas Reservoirs*. Paper presented at the CPS/SPE International Oil & Gas Conference and Exhibition in China, Beijing, China.

Rapoport, L. A., & Leas, W. J. (1953). Properties of Linear Waterfloods. *Society of Petroleum Engineers*. doi:10.2118/213-G

Ribeiro, L. H., & Sharma, M. M. (2012). Multi-phase Fluid-Loss Properties and Return Permeability of Energized Fracturing Fluids. *Society of Petroleum Engineers*. doi:10.2118/139622-PA

Richardson, J. G., Kerver, J. K., Hafford, J. A., & Osoba, J. S. (1952). Laboratory Determination of Relative Permeability. *Society of Petroleum Engineers*. doi:10.2118/952187-G

Ruppert, L. F., Sakurovs, R., Blach, T. P., He, L., Melnichenko, Y. B., Mildner, D. F. R., & Alcantar-Lopez, L. (2013). A USANS/SANS Study of the Accessibility of Pores in the Barnett Shale to Methane and Water. *Energy & Fuels, 27*(2), 772-779. doi:10.1021/ef301859s

Sharma, M. M., & Manchanda, R. (2015). *The Role of Induced Un-propped (IU) Fractures in Unconventional Oil and Gas Wells*. Paper presented at the SPE Annual Technical Conference and Exhibition, Houston, Texas, USA.

Sigal, R. F. (2015). Pore-Size Distributions for Organic-Shale-Reservoir Rocks From Nuclear-Magnetic-Resonance Spectra Combined With Adsorption Measurements. *Society of Petroleum Engineers*. doi:10.2118/174546-PA

Soni, T. M. (2014). *LPG-Based Fracturing: An Alternate Fracturing Technique in Shale Reservoirs*. Paper presented at the Asia Pacific Drilling Technology Conference, Bangkok, Thailand.

Spencer, C. W. (1989). Review of characteristics of low-permeability gas reservoirs in western United States. *AAPG bulletin, 73*(5), 613-629.

Tavassoli, Z., Zimmerman, R. W., & Blunt, M. J. (2005). Analytic Analysis for Oil Recovery During Counter-Current Imbibition in Strongly Water-Wet Systems. *Transport in Porous Media, 58*(1), 173-189. doi:10.1007/s11242-004-5474-4